*molecules*

MDPI

*Review*

# Synthesis and Application of LTA Zeolite for the Removal of Inorganic and Organic Hazardous Substances from Water: A Review

**Junyao Pan, Binyu Wang, Simiao Liu, Shanshan Liu and Wenfu Yan ***

State Key Laboratory of Inorganic Synthesis and Preparative Chemistry, College of Chemistry, Jilin University, Changchun 130012, China; pjy23@mails.jlu.edu.cn (J.P.); wangbinyu@ciomp.ac.cn (B.W.); 15143706097@163.com (S.L.); 15713854388@163.com (S.L.)
* Correspondence: yanw@jlu.edu.cn

**Abstract:** Industrialization and human activities have caused significant environmental challenges, with water pollution posing severe risks to human health. This underscores the urgent need for effective water treatment solutions. Zeolites, known for their high specific surface area and stability, have gained increasing attention as adsorbents for water treatment. Among zeolites, **LTA** varieties stand out due to their low Si/Al ratio, which enhances ion-exchange capacity, and their cost-effectiveness. This review focuses on the synthesis of low-silica **LTA** zeolites, particularly zeolite A, using natural materials and solid wastes without relying on organic-structure-directing agents (OSDAs). Common pretreatment processes for such synthesis are also highlighted. The review further explores the applications of **LTA** zeolites in water treatment, emphasizing their exceptional performance in adsorbing inorganic and organic pollutants. In particular, **LTA** zeolites are highly effective at removing inorganic cation pollutants through ion exchange. An updated ion-exchange selectivity order, based on previous studies, is provided to support these findings. Overall, this review aims to guide future research and development in water treatment technologies.

**Keywords:** **LTA** zeolite; solid waste; water treatment; heavy metal; ion-exchange selectivity order

check for updates

Academic Editor: Łukasz Kuterasiński

Received: 24 December 2024
Revised: 22 January 2025
Accepted: 23 January 2025
Published: 25 January 2025

**Citation:** Pan, J.; Wang, B.; Liu, S.; Liu, S.; Yan, W. Synthesis and Application of LTA Zeolite for the Removal of Inorganic and Organic Hazardous Substances from Water: A Review. *Molecules* **2025**, *30*, 554. https://doi.org/10.3390/molecules30030554

**Copyright:** © 2025 by the authors. Licensee MDPI, Basel, Switzerland. This article is an open access article distributed under the terms and conditions of the Creative Commons Attribution (CC BY) license (https://creativecommons.org/licenses/by/4.0/).

## 1. Introduction

As industrialization intensifies and human civilization advances, pollution from human activities has become widespread. Among various forms of pollution, water contamination is particularly concerning due to its direct impacts on ecosystems and human health [1–7]. Industrial processes, such as metal plating, metallurgy, petroleum refining, battery production, mining, textiles, and pharmaceuticals, generate waste that is often discharged into groundwater, rivers, and lakes, posing significant risks [8–10]. Water pollutants include heavy metal ions (e.g., lead, cadmium, copper, zinc, and nickel), harmful anions (e.g., arsenate, chromate, fluoride, and phosphate), organic dyes, and pharmaceutical compounds [11,12]. This underscores the urgent need for effective wastewater treatment methods to meet safety standards and restore contaminated water systems.

The diverse nature of water pollutants poses significant challenges for effective treatment. Conventional methods such as membrane filtration, chemical oxidation, solvent extraction, adsorption, coagulation, flocculation, and biological treatment have notable limitations [13–20]. Many of these techniques rely heavily on chemicals, including chlorides,

ammonia, permanganate, alum, sodium hydroxide, hydrochloric acid, ozone, and iron salts. Additionally, they require complex mechanical processes, substantial engineering expertise, and advanced infrastructure [21]. Tailoring individual treatments for each pollutant is often impractical, as traditional technologies are frequently unable to completely remove toxins, phosphorus, nitrogen, and heavy metals [22,23]. In contrast, adsorption offers a simpler, cost-effective, and efficient approach that avoids generating secondary pollution [24]. However, a key challenge in adsorption is the development of adsorbents with high capacity, rapid kinetics, superior selectivity, and excellent recyclability [25].

Zeolites, inorganic porous aluminosilicates, are particularly well-suited for wastewater treatment due to their outstanding thermal and chemical stability. Their high specific surface area, tunable pore structures, and abundant ion-exchange sites enable the efficient removal of toxic substances, including heavy metal ions, from water [25–29]. Both natural and synthetic zeolites have been extensively studied and proven effective for water pollutant adsorption [30–34]. Since 2010, research on zeolite-based adsorbents has grown significantly, emphasizing their potential in mitigating water pollution (Figure 1) [35]. Although the overall number of publications on wastewater adsorption declined between 2022 and 2024, studies focusing on zeolite-based adsorbents consistently accounted for approximately 9% of the total research output.

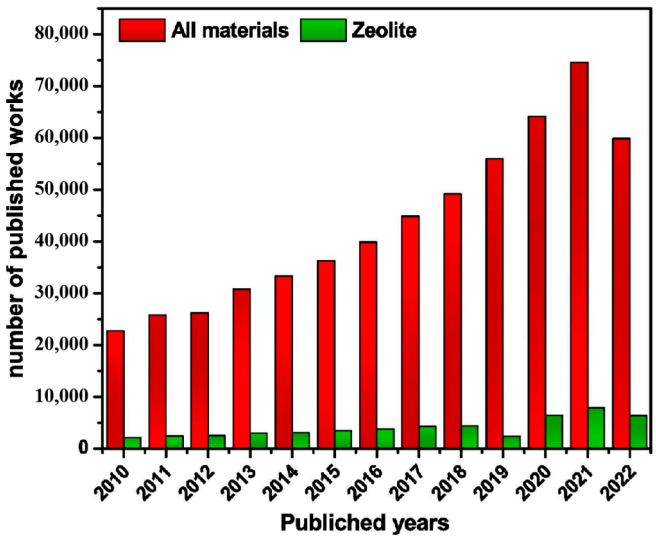



**Figure 1.** Evolution of the number of works published on the adsorption of wastewater pollutants. Reprinted with permission from Ref. [35]. Copyright (2024) Elsevier.

The Structural Committee of the International Zeolite Association (IZA-SC) currently recognizes over 260 zeolite structures [36]. Among these, zeolite A (Linde type A or **LTA**) is notable as the first commercially synthetized zeolite and is widely used as a gas adsorbent and ion exchanger [37]. While many **LTA** zeolites have been developed with Si/Al ratios (SAR) greater than 1 [38–43], OSDA-free zeolite A remains a popular choice for water treatment. Its low Si/Al ratio (SAR = 1) provides abundant $[AlO_4]^-$ sites for ion exchange, resulting in a high adsorption capacity [44]. Additionally, the three-dimensional channels in **LTA** zeolites facilitate rapid ion migration, enabling fast adsorption kinetics. Due to its simple, low-cost, and efficient synthesis, zeolite A remains a leading material for water treatment applications.

This review examines research published since 1995, with a focus on studies from 2010 onward, regarding the synthesis and application of zeolite A in water treatment. We highlight works that emphasize novel synthesis methods or materials demonstrating exceptional water treatment performance. Specifically, we explore advancements in low-

cost, environmentally friendly production methods using natural resources and solid waste. The applications of zeolite A and its composites for adsorbing hazardous substances in aqueous solutions are also discussed. An updated ion-exchange selectivity order is provided, encompassing all inorganic cations that can exchange into zeolite A—an aspect not covered in previous reviews. Finally, we present perspectives on the future of zeolite-based water treatment, aiming to guide further research and development. This review serves as a valuable resource for researchers and professionals working in the field of water treatment.

## 2. Zeolite A and Its Synthesis

Zeolites were first identified in volcanic rocks by Swedish mineralogist Axel Fredrik Cronstedt, who observed that they released water vapor upon heating, resembling boiling. This phenomenon inspired the name "zeolite". Zeolites are three-dimensional frameworks with uniform, molecular-sized pores, often referred to as molecular sieves. Their structure consists of interconnected $TO_4$ tetrahedra (where T represents Si or Al), linked by oxygen atoms. The negative charge from $[AlO_4]^-$ units in the framework is balanced by positive cations located within the pores (Figure 2) [45]. The general empirical formula for zeolites is $M_{x/n}[(AlO_2)_x(SiO_2)_y]\cdot wH_2O$, where M is an extra-framework cation with valence n, y/x represents the Si/Al ratio, and w denotes the number of water molecules.

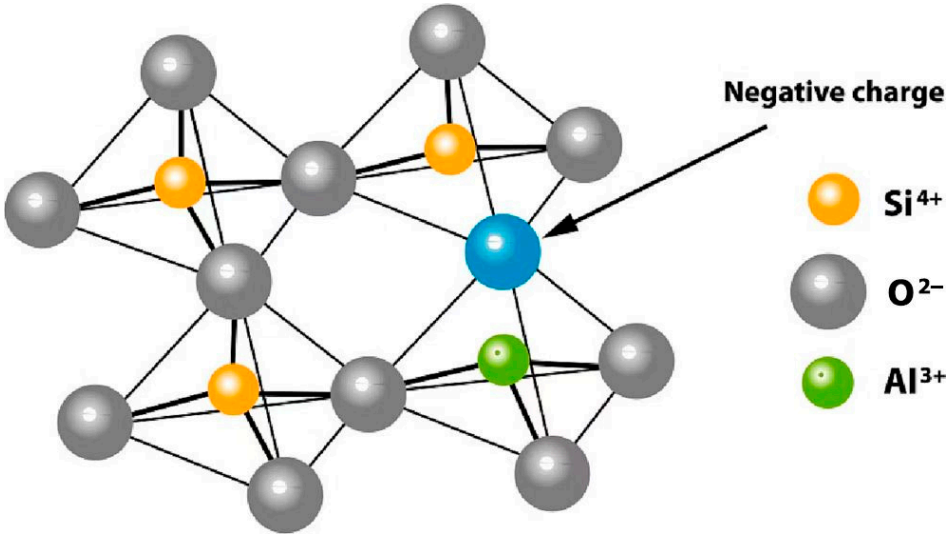



**Figure 2.** Structure of zeolite **LTA** (source: International Zeolite Association (IZA)). Reprinted with permission from Ref. [45]. Copyright (2023) Elsevier.

Since the 1950s, zeolites have been widely used in various applications. Natural zeolites, formed by the interaction of volcanic rocks and ash with alkaline groundwater, are often impure and therefore rarely used commercially. In contrast, synthetic zeolites are extensively employed in water treatment, gas separation, and catalysis. They serve as ion exchangers, adsorbents, and solid acid catalysts, demonstrating versatility and effectiveness across multiple industries [46–48].

Zeolite A was the first synthetic zeolite to be commercialized [49]. In its $Na^+$-exchanged form, it has the formula $Na_{12}[(AlO_2)_{12}(SiO_2)_{12}]\cdot 27H_2O$, with an Si/Al ratio of 1—the lowest among aluminosilicate zeolites. The $Na^+$ ions within the structure are readily exchangeable [50]. The framework of zeolite A consists of two types of cages: $\alpha$-cages and $\beta$-cages (also known as sodalite cages). Sodalite cages are connected through double four-membered rings (D4Rs), creating a three-dimensional network [37]. Eight sodalite cages fused by D4Rs form a larger $\alpha$-supercage (Figure 3a). The type of cation present (e.g., $K^+$,

$Na^+$, or $Ca^{2+}$) influences the average channel size, leading to different zeolite designations: 3A, 4A, and 5A, respectively [51]. Zeolite A crystals typically exhibit a sharp-edged cubic morphology, as illustrated in Figure 3b,c.

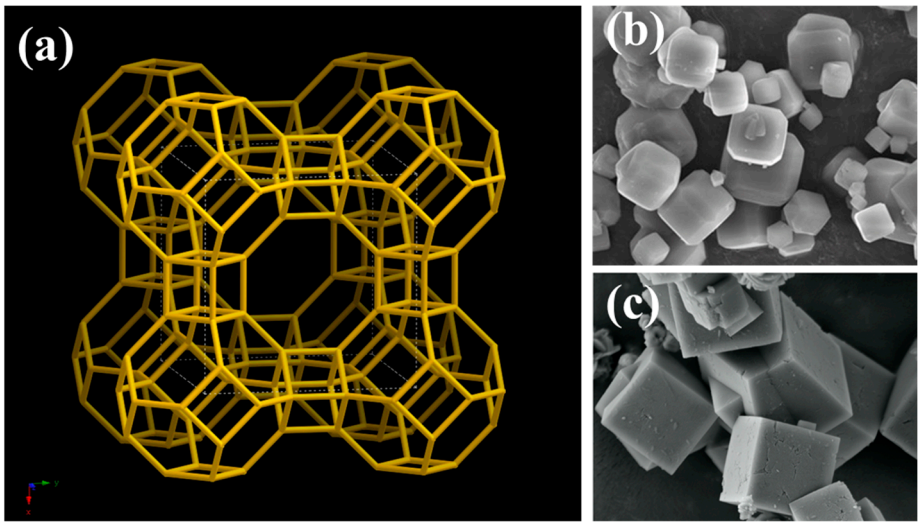



**Figure 3.** (**a**) Structure of zeolite **LTA** (source: International Zeolite Association (IZA)). (**b**,**c**) SEM images of zeolite A. Reprinted with permission from Refs. [52,53]. Copyright (2018) MDPI and (2024) MDPI.

Commercially, zeolite A is synthesized with an Si/Al ratio of approximately 1, resulting in a high density of cation-exchange sites. This property makes it a highly effective adsorbent for water pollution treatment.

### *2.1. Synthesis of Low-Silica LTA from Pure Chemical Raw Materials*

Zeolite A can be synthesized using various silicon and aluminum sources through different processes [54–58]. Typically, the synthesis involves mixing an alkaline solution of silicon and aluminum sources to form aluminosilicate gels, followed by hydrothermal treatment at approximately 100 °C to crystallize zeolite A. Key parameters—such as temperature, crystallization time, pH, mixing sequence, and raw material type—significantly influence the synthesis outcome [59–61].

For example, Wang et al. studied the effects of inorganic anions on zeolite A synthesis [62]. They observed that $Na_2CO_3$ increased the dissolution rate of zeolite A but had a minimal impact on sodalite crystallization. $Na_3PO_4$ inhibited sodalite crystallization, while $Na_2SO_4$ promoted sodalite formation and improved particle size. Notably, $SO_4^{2-}$ containing sodalite had a larger unit cell compared to other sodalite types. These findings indicate that $CO_3^{2-}$ and $SO_4^{2-}$ destabilize **LTA** phases, whereas $PO_4^{3-}$ has a stabilizing effect.

Efforts to reduce crystallization temperatures and times have shown promising results. Jafari et al. synthesized zeolite A at 60 °C using aluminum isopropoxide, colloidal silica, and sodium hydroxide [63]. Similarly, Huang et al. produced single crystals and nanocrystal aggregates near room temperature [64]. Zhang et al. synthesized zeolite A at room temperature using various silicon sources (e.g., fumed silica, water glass) and aluminum sources (e.g., aluminum isopropoxide, aluminum powder), though this extended the crystallization times significantly [65]. Sun et al. improved this process, achieving zeolite A in 4 h using atmospheric reflux [66]. Furthermore, advanced techniques such as microwave and ultrasound methods have been used to accelerate crystallization [67–69].

Crystal size plays a crucial factor in the performance of zeolite A. Sharma et al. synthesized thermally stable nanocrystals through hydrothermal treatment of ammonium aluminate and sodium silicate at 100 °C for 24 h, with the resulting crystals maintain-

ing structural integrity up to 1000 °C [70]. Fang et al. created submicron zeolite A on a honeycomb ceramic matrix using microwave hydrothermal methods [71]. Mintova et al. demonstrated that ageing amorphous gels for 3 d before hydrothermal treatment enhanced crystal nucleation and growth [72].

Factors such as alkalinity, hydrothermal conditions, and ageing also affect crystal size. Yu et al. found that higher sodium concentrations resulted in larger crystals, while prolonged ageing reduced crystal size and improved uniformity [73]. Bayati et al. reported that higher crystallization temperatures and extended times generally produced larger particles, with temperature having a more significant impact than time [74].

To address diffusion limitations within microporous **LTA** channels, researchers have developed hierarchical zeolite A structures with mesoporosity [75–79]. For example, Chen et al. used three-dimensionally ordered mesoporous carbon as a template to create mesoporous zeolite A [80]. Cho et al. introduced organosilane surfactants into the synthesis mixture to form mesopores [81]. Hasan et al. utilized cetyltrimethylammonium bromide to produce hierarchical zeolite A and synthesized core–shell structures with hollow morphologies through a two-step crystallization process [82,83].

For practical applications, zeolite A often requires granulation to improve mechanical strength. However, traditional binders can reduce its specific surface area and porosity [84,85]. To address this, binder-free microspheres have been developed. Yu et al. created zeolite A/chitosan hybrid microspheres using biomolecules [86], while others incorporated clay during hydrothermal synthesis to produce binder-free zeolite A [87].

### *2.2. Synthesis of Low-Silica LTA from Natural Substances and Solid Waste*

Research on synthesizing zeolite A from natural substances and solid waste is primarily conducted at the laboratory scale. The industrial process involves two main stages: raw material activation and product crystallization (Figure 4). Activation methods include high-temperature roasting, acid treatment, and high-temperature solid-phase alkali fusion. The choice of activation method depends on the raw material composition and is tailored accordingly [88–91].

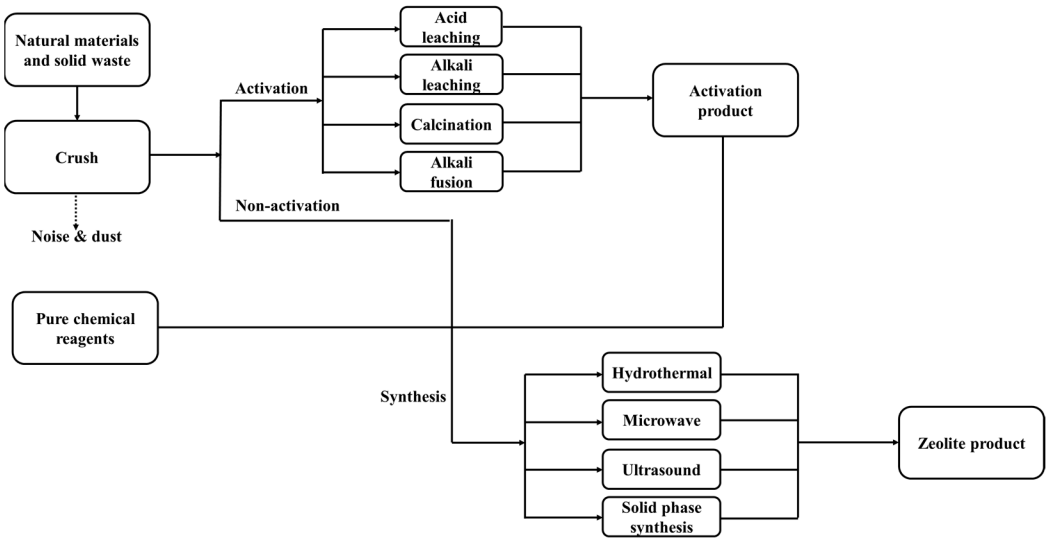



**Figure 4.** Flow chart of zeolite synthesis from natural materials and solid waste.

#### 2.2.1. Coal Fly Ash (CFA)

Coal fly ash (CFA) is generated during coal combustion at temperatures between 1300 and 1500 °C, producing small spherical particles with smooth surfaces and fine micropores [92]. Power plants produce vast amounts of fly ash, exceeding 800 million

tonnes annually, with the largest contributions from China, India, and the USA. CFA is a valuable source of silicon, containing high silicon content along with smaller amounts of aluminum, iron, calcium, magnesium, and potassium [93,94]. Despite its potential, a significant portion of CFA is still treated as waste and remains underutilized [95,96].

Research on zeolite synthesis from CFA highlights the importance of the pretreatment process, such as alkali fusion activation. In some cases, acid leaching is also required to extract active Si and Al while minimizing interference from impurities like Fe and mullite [97,98]. For instance, Cao et al. synthesized zeolite A by calcining CFA at 750 °C for 3 h [99]. Similarly, Fan et al. used CFA calcined at 700 °C for 3 h to prepare zeolite A [100]. Yang et al. investigated the effects of NaOH and $Na_2CO_3$ on CFA activation for synthesizing zeolite 4A [101]. They found that using $Na_2CO_3$ alone produced zeolite 4A with slightly higher crystallinity but required a higher alkali dosage. However, mixing $Na_2CO_3$ and NaOH in a 2.8:1 mass ratio yielded zeolite 4A with the highest crystallinity (75.8%) under conditions of low energy and water consumption. In other studies, Nowak et al. synthesized zeolite A from low-quality CFA and wet flue gas desulphurization wastewater [102], while Kunecki et al. optimized activation conditions to 550 °C for 1 h [103].

In addition to solid-phase activation, liquid-phase methods have been developed for synthesizing zeolite A from CFA. These methods typically require milder conditions, making them more cost-effective and safer. For example, Chareonpanich et al. activated CFA by dispersing it in sodium hydroxide solution, heating it at 120 °C for 4 h, and synthesizing zeolite A in an integrated process [104]. This approach simplifies operations by reducing the need for specialized equipment, such as Teflon-lined autoclaves. Due to variations in coal composition from different sources, tailored preparation strategies are often necessary for synthesizing zeolite **LTA** [37].

#### 2.2.2. Kaolin and Clay

Kaolin clay ($Al_2Si_2O_3(OH)_4$) is a significant source of silica and alumina for the synthesis of zeolite A. Numerous studies have employed kaolin as a feedstock for zeolite A production [105–107]. When calcined at temperatures between 550 and 900 °C, kaolin transforms into reactive metakaolin [108].

Holmes et al. calcined Nigerian kaolin at 650 °C for 10 min to produce metakaolin. However, the sample retained quartz, which limited the quality of the synthesized zeolite A despite attempts to remove impurities [109]. In contrast, Schwanke et al. successfully synthesized antibacterial zeolite A using Brazilian Amazon kaolin mining waste. The waste was calcined at 600 °C for 2 h to form metakaolin [110]. Wang et al. synthesized flaky zeolite NaA with kaolin as the sole source of Si and Al, achieving a specific surface area of 39.8 $m^2 \cdot g^{-1}$, mainly mesoporous. This was significantly higher than that of the surface area of traditional NaA [111].

Efforts to simplify and create milder pretreatment methods for zeolite synthesis have increased. Wang et al. proposed an approach that bypasses calcination by directly reacting natural kaolin with NaOH to hydrothermally [112]. This forms hydrous sodium aluminosilicates, which are then dissolved in dilute HCl to yield an amorphous Si-Al gel. The gel is suitable for hydrothermal synthesis of zeolite A. Compared to conventional calcination methods, this process offers better control over particle size and morphology, resulting in enhanced brightness and cation-exchange capacity.

Microwave-assisted synthesis has emerged as an alternative to traditional hydrothermal methods, as it has improved energy conduction, leading to smaller and more uniform zeolites [113]. Oliveira et al. converted metakaolin into zeolite A using microwave-assisted techniques, achieving excellent $CO_2$ adsorption capacity [114]. Similarly, Chen et al. ob-

served that microwave radiation reduced activation energy and accelerated crystallization during kaolin calcination and 4A zeolite synthesis [115].

Solvent-free methods have also gained attention. Yang et al. developed a solvent-free strategy to prepare self-supporting hierarchical porous zeolites, using polymethyl methacrylate (PMMA) microspheres as sacrificial templates [116].

Beyond kaolin, other natural clays can also serve as effective raw materials for zeolite A synthesis. Si et al. synthesized zeolite A from spherical clay calcined at 600 °C and crystallized at 60 °C for 48 h [117]. García et al. also prepared zeolite A with excellent optical properties using natural clay [118]. Foroughi et al. explored the effects of clay type on product morphology during zeolite A synthesis [119]. Zeolite A synthesized from a clay mixture containing illite, kaolinite, and pyrophyllite exhibited semi-cubic particles with rounded edges and a lower surface area (17.5 $m^2 \cdot g^{-1}$). In contrast, products synthesized from kaolinite-rich clay were mesoporous, with an average pore size of 8 nm and a larger surface area (~59.6 $m^2 \cdot g^{-1}$).

#### 2.2.3. Coal Gangue

Coal gangue (CG), a hazardous by-product of coal mining, constitutes approximately 10–15% of raw coal production. Its massive accumulation presents significant environmental challenges worldwide [120]. However, CG is rich in $SiO_2$ and $Al_2O_3$, making it a valuable resource for zeolite synthesis and an environmentally friendly application for waste management.

Several studies have explored methods for synthesizing zeolite A from CG. Qian et al. and Wang et al. adopted an in situ synthesis method, which involved calcining CG for decarburization, followed by melting with NaOH at 400–500 °C for 2 h [44,121]. Liu et al. developed a two-step synthesis process to produce high-whiteness zeolite A. This approach included high-temperature calcinations to reduce $Fe_2O_3$ content, followed by hydrothermal acid leaching to remove Fe impurities and enhance ion-exchange capacity [122]. Similarly, Kong et al. utilized a pretreatment of calcination, acid leaching and alkali fusion to synthesize zeolite A from high-iron, high-quartz CG [123].

Recently, simplified methods have emerged that omit some pretreatment steps beyond calcination, streamlining the zeolite A synthesis process from CG [124–126].

#### 2.2.4. Rice Husk Ash and Other Biomass Ash

Rice husk ash (RHA), a by-product of rice processing, contains more than 90% silica, which can exist in crystalline or amorphous forms depending on combustion conditions [127,128]. Its low cost and wide availability make RHA an attractive raw material for zeolite A synthesis.

The typical synthesis process involves calcining rice husk at approximately 700 °C to produce RHA. This ash is then activated with sodium hydroxide to extract silica as a soluble silica sol. Acid leaching with HCl or $HNO_3$ may be used to precipitate impurities, yielding a purified silica gel for zeolite synthesis [129–131]. For example, Madhu et al. synthesized zeolite A with high $CO_2$ adsorption performance by extracting $SiO_2$ from RHA with NaOH [132]. Ghasemi et al. enhanced the process by using HCl to remove impurities prior calcination [133].

Schmitz et al. investigated the impact of different RHA sources on zeolite A synthesis. They found that the proportion of amorphous silica in RHA significantly influences its solubility in NaOH, which affects the crystallization process [129]. Amorphous silica obtained through controlled calcination typically produces larger crystals and better intergrowth of cubic crystals compared to commercial fumed silica. Tan et al. examined how calcination temperature and duration affect RHA composition and zeolite morphology [134]. They

observed that RHA calcined at higher temperatures and for longer durations develops a porous structure, enhancing solubility and reaction efficiency. Nawog et al. simplified the process by synthesizing nano-NaA zeolites directly from RHA without silica extraction or the use of OSDAs, reducing solvent and reagent consumption [135].

Other biomass ash sources, such as sugarcane bagasse ash [136], barley husk [137], wheat husk [138], date leaf midribs [139], phragmites australis [140], and bamboo leaf [141], have also been explored for zeolite A synthesis. For instance, Küçük et al. utilized biomass fly ash from a co-incineration plant at a paper mill to synthesize zeolite A [142]. Azizi et al. synthesized zeolite A from barley husk, using NaOH pretreatment to extract silica [143]. Moisés et al. optimized silica utilization by combining sugarcane bagasse ash with solid NaOH, melting the mixture at 550 °C and subsequently adding water to prepare a sodium silicate solution for zeolite A synthesis [144].

#### 2.2.5. Diatomite

Diatomite, also known as diatomaceous earth, is a sedimentary rock composed of fossilized single-celled algae [145]. Its primary component is amorphous silica or hydrated opaline silica, valued for its chemical stability and inertness. Diatomite is widely used in filtration and adsorption applications, such as managing organic waste in the food industry [146,147]. Recycling diatomite into value-added products offers both environmental and economic benefits.

Recent studies have explored diatomite as a raw material for zeolite synthesis. For example, Nascimento et al. synthesized zeolite A from diatomite with a silicon–aluminum ratio of approximately 1–2 [148]. El-Kordy et al. developed zeolite A–clay composites using diatomite combined with natural clay [149].

#### 2.2.6. Mineral Waste Residue

Mineral waste residue, generated during mining and mineral extraction, can pose environmental hazards if improperly managed. However, slag containing high levels of Si or Al offers a cost-effective and sustainable option for zeolite synthesis.

Li et al. synthesized highly crystalline zeolite A from calcined lithium slag at a low temperature of 60 °C [150]. Wu et al. utilized calcined and HCl-leached opal waste, achieving zeolite A with excellent ammonium exchange capacity [151]. Lei et al. activated bauxite tailings via alkali fusion at 500 °C for 3 h to produce zeolite A [152]. Yan et al. created magnetic zeolite A from red mud and coal gangue using an alkali-reducing calcination-hydrothermal method [153]. Kuroki et al. prepared zeolite A by reacting crushed stone powder with aluminum ash following alkali and acid treatments [154].

#### 2.2.7. Waste Glass and Sand

Waste glass, commonly sourced from beverage bottles, windscreens, and television panels, is often recycled. However, conventional recycling methods require heating to around 1500 °C, leading to high energy consumption and significant greenhouse gas emissions [155].

Yao et al. synthesized zeolite A from waste cathode ray tubes, examining the effects of hydrothermal temperature and the $SiO_2/Al_2O_3$ ratio on the final product [156]. At lower temperatures (80–100 °C) and pressure (0.47–1.01 bar), and at an $SiO_2/Al_2O_3$ ratio of 2.0, amorphous phases were observed. Increasing the temperature to 110 °C and pressure to 1.43 bar yielded NaA zeolite, along with NaP1 and Faujasite. Higher temperatures and pressures caused NaA and Faujasite to disappear, with hydroxysodalite becoming the dominant phase. The $SiO_2/Al_2O_3$ ratio also influenced the phases formed: a ratio of 1.5 produced pure NaA, while a ratio of 2.0 led to a mixture of NaA and Faujasite. Lee et al. used waste glass from liquid crystal displays (LCDs) and sandblasting waste to synthesize

zeolite A, optimizing the process to achieve superior water adsorption and desorption properties [157]. Similarly, Prasertsab et al. synthesized zeolites **LTA** and **FAU** from waste sand generated during oil and gas production [158].

#### 2.2.8. Aluminum Waste

Aluminum is an essential metal in various industries, including aerospace, automotive, food and beverage, construction, and electrical/electronics. Consequently, large amounts of aluminum waste are generated, particularly from beverage cans, highlighting the need for sustainable recycling and reuse methods.

Terzano et al. synthesized zeolite A from municipal glass and aluminum wastes using a one-pot process without prior activation [155]. Tounsi et al. prepared zeolite A by reacting sodium silicate, extracted from Tunisian sand, with aluminum scrap dissolved in NaOH [159]. Similarly, Abdelrahman dissolved aluminum cans in NaOH, filtered out impurities, and synthesized zeolite A using various silicon sources, including fumed silica, sodium metasilicate, silica sol, and tetraethyl orthosilicate [160].

#### 2.2.9. Furnace Slag

Furnace slag is a by-product of the iron smelting industry and is primarily composed of Si, with notable amounts of Al, Ca, Mg, and other metals [161].

Sugano and Murakami attempted to synthesize zeolite A directly from blast furnace slag, but the resulting product had low purity, with only 60% zeolite A content [162,163]. They identified that the presence of Ca and Mg oxides hindered zeolite A crystallization. To address this, Anuwattana proposed a method involving calcination followed by acid pickling to remove these impurities, improving the synthesis of zeolite A [164]. Similarly, Li et al. used co-calcination of blast furnace slag with NaOH to produce zeolite A [165].

Linz–Donawitz (LD) slag is generated during the conversion of pig iron to crude steel in the Linz–Donawitz process [166]. Samanta et al. synthesized zeolite A from LD slag and evaluated its ability to remove $Fe^{3+}$ ions and the cationic dye methylene blue, as discussed in the next section [167,168]. The activation process for LD slag included calcination, acid pickling, and alkali fusion activation.

#### 2.2.10. Natural Zeolites

Natural zeolites have been used for centuries, but their impurities and low crystallinity limit their industrial applications [169,170]. Despite this, the high Si and Al content of natural zeolites, along with their zeolite phases, has attracted significant interest in synthesizing more effective synthetic zeolites from these materials.

For example, Faghihian et al. synthesized zeolite A from natural clinoptilolite through an interzeolite transformation method after refluxing the material for 3 days [171,172]. Similarly, Kazemian et al. transformed natural clinoptilolite into zeolite A without the need for activation [173]. Yue et al. produced high-purity zeolite A from natural stellerite sourced from Gongxi, China, by co-calcination with $Na_2CO_3$ at temperatures between 700 and 900 °C [174].

#### 2.2.11. Spent FCC Catalysts

The fluid catalytic cracking (FCC) process is essential in petroleum refineries, particularly for gasoline production [175]. Catalysts facilitate the cracking of hydrocarbons to yield valuable products. However, this process generates coke, which deposits on the catalyst's active sites, leading to deactivation. Additionally, metals such as vanadium (V), iron (Fe), and nickel (Ni) can accumulate on the catalyst surface, further contributing to deactivation [176].

The FCC process generates substantial amounts of spent catalysts, which mainly consist of ZSM-5, zeolite Y, and various alumina substrates. These spent catalysts may also contain toxic metals like V, Fe, and Ni, as well as rare earth metals such as lanthanum (La) and cerium (Ce). Gonzalez et al. synthesized zeolite A from waste FCC catalysts without activation, although the conversion efficiency of the raw materials needed improvement [177]. They later proposed a high-temperature alkali fusion activation method to enhance conversion [178]. Monzón et al. employed a similar method and achieved zeolite A with good crystallinity [179].

To reduce energy consumption and improve safety, Wang et al. introduced a low-temperature (200 °C) alkali fusion activation method for synthesizing zeolite A (designated as SFCC-A) from waste FCC catalysts [33]. The resulting SFCC-A exhibited crystallinity and ion adsorption capacities comparable to commercial zeolite A.

#### 2.2.12. Waste Ceramics

The ceramic industry generates significant amounts of waste ceramics, primarily in the form of silicon-based materials, which can potentially be converted into zeolites [180]. This conversion offers an opportunity to recycle waste ceramics, contributing to sustainability and resource efficiency within the industry.

Wajima et al. developed a method to extract silica from waste ceramics using NaOH solution, subsequently synthesizing zeolite A from the recovered silica [181]. The silica recovery rate achieved was an impressive 26,000 mg/L. This approach has since been adopted by other researchers to convert waste ceramics into zeolite A [182].

#### 2.2.13. Electrolytic Manganese Residue

Electrolytic manganese residue (EMR) is a by-product generated during the solid-liquid separation step in the acid leaching of manganese ore to prepare electrolytes. EMR presents significant environmental challenges and incurs high treatment costs, limiting the sustainable development of manganese metallurgy.

The components of EMR vary depending on their source but typically consist predominantly of silica [183]. Li et al. utilized EMR to synthesize zeolite A for the adsorption of inorganic cationic pollutants [184–186]. Their process involved alkali fusion activation at 800 °C, followed by ageing the product in deionized water. The activated material was filtered, and the resulting filtrate was used for hydrothermal synthesis.

#### 2.2.14. Other Raw Materials

In addition to the materials mentioned above, several natural and waste-derived substances have been explored as precursors for zeolite A synthesis. These include natural materials such as perlite [187], volcanic ash [188], halloysite [189,190], and oil shale [191]. Solid waste sources, such as waste incineration fly ash [192,193], red mud [194], waste peat ash [195], coal gasification slag [196], tannery wastewater [197], and foundry dust [198], have also been effectively utilized.

### *2.3. Synthesis of High/Pure Silica LTA*

The first pure silica **LTA** zeolite, known as ITQ-29, was synthesized using fluoride media in conjunction with methylated julolidine and tetramethylammonium ($TMA^+$) as OSDAs [199]. Since then, efforts have focused on developing ITQ-29 using alternative OSDAs. Tiscornia et al. synthesized ITQ-29 membranes on alumina tubular supports using a supramolecular molecule along with $TMA^+$ [42]. Boal et al. introduced a novel imidazolium-based OSDA, which, when used combined with $TMA^+$ as a co-OSDA, optimized the synthesis of ITQ-29 [200]. Their method also enabled the production of high-silica and silicogermanium variants of **LTA** zeolites with Si/Al ratios ranging from 12 to 42.

Imidazolium-based ITQ-29 seeds were employed to achieve these results (Figure 5). This strategy has since been widely adopted for synthesizing high-silica **LTA** zeolites.

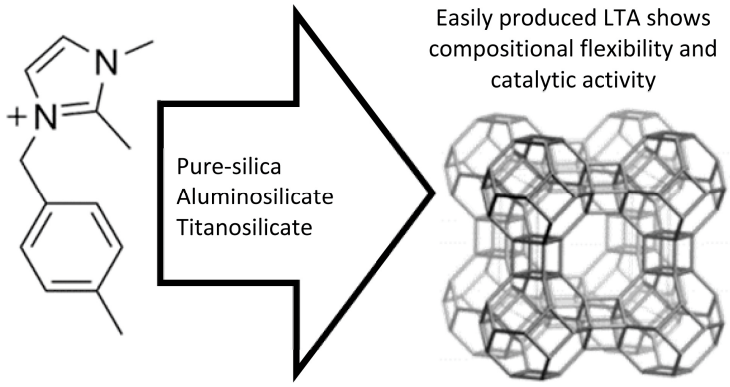



**Figure 5.** Imidazolium OSDA for the synthesis of ITQ-29 and high-silica **LTA** zeolites. Reprinted with permission from Ref. [200]. Copyright (2015) ACS.

Previously, zeolite A with an Si/Al ratio greater than 1 (known as ZK-4) was typically synthesized using TMAOH as the OSDA in potassium ($K^+$)-mediated systems [38–40,43,201,202]. However, these methods rarely produced zeolites with Si/Al ratios exceeding 3. Tao et al. successfully synthesized high-silica **LTA** zeolites with an Si/Al ratio of 6 by using tetramethylammonium, tetraethylammonium, and dimethyldiethylammonium as co-OSDAs [203]. The introduction of imidazolium-based OSDAs further advanced the synthesis of **LTA** zeolites, enabling Si/Al ratios of 10 or even higher. Hong's group leveraged this approach to synthesize a series of high-silica **LTA** zeolites for applications such as $NH_3$-SCR [204–208].

### *2.4. Synthesis of AlPO/SAPO LTA*

The zeolite A variant AlPO/SAPO is also known as AlPO-42/SAPO-42. Its synthesis typically requires a fluoride ($F^-$) introduction system, as reported in recent studies [209–212]. Similar to the synthesis of high/pure silica **LTA** and silicogermanium **LTA**, aluminophosphate-based **LTA** can be synthesized using $TMA^+$ and rigid imidazole-based molecules as OSDAs.

In 2010, Huang et al. synthesized large single crystals of AlPO-LTA using the crown ether Kryptofix 222 as an OSDA [213]. Azim et al. employed 1-butylpiperidine chloride in an ionothermal method to produce AlPO-42 [214]. Xu et al. used n-propylamine as an OSDA to hydrothermally synthesize large single crystals of AlPO-42 [215]. Lin et al. utilized 1-ethyl-3-methyl imidazolium bromide with tetraalkylammonium ionic liquid in ionothermal synthesis [210]. AlPO-42 has also been synthesized using co-OSDAs, including 1-butyl-3-methylimidazolium bromide and $TMA^+$ as co-OSDAs [209,211,212].

For SAPO-42, Pinilla-Herrero et al. demonstrated the use of $TMA^+$ and diethanolamine (DEA) as co-OSDAs [216,217]. Lin et al. and Vinaches et al. synthesized SAPO-42 using imidazole-based OSDAs under ionothermal and hydrothermal conditions, respectively [218,219]. Additionally, Martínez-Franco et al. developed two self-assembled aromatic molecules—2,2-dimethyl-2,3-dihydro-1H-benzo[de]isoquinoline-2-ium and 4-methyl-2,3,6,7-tetrahydro-1H,5H-pyrido[3.2.1-ij]quinolinium as OSDA for SAPO-42 synthesis. These strategies pave the way for synthesizing aluminophosphate-based and high-silicon **LTA** [220].

## 3. Removal of Hazardous Substances from Water by Zeolite A

Zeolite A and its composites have been widely studied for removing hazardous substances from water. These studies primarily target inorganic cation pollutants, including toxic heavy metals, simulated radionuclides, water-softening ions such as $Mg^{2+}$ and $Ca^{2+}$, and ammonia nitrogen. Some research also addresses the removal of organic pollutants, such as dyes and pharmaceuticals. Zeolite A demonstrates high adsorption capacities for most metal cations, as summarized in Table 1. For example, $Sr^{2+}$ adsorption capacity reaches 294.1 $mg \cdot g^{-1}$, while $Pb^{2+}$ achieves 880 $mg \cdot g^{-1}$. The adsorption of cationic pollutants is generally described by the Langmuir isotherm and pseudo-second-order kinetic models, highlighting ion exchange as the primary mechanism. In modified zeolite A, alternative models such as the Friedrich isotherm and pseudo-first-order kinetics may apply due to structural changes affecting adsorption behavior.

### *3.1. Removal of Heavy Metal Cations*

The rapid pace of industrialization, coupled with human activities such as mining and waste generation, has led to a significant increase in heavy metal pollution. Industrial waste containing heavy metals contaminates the environment, posing severe health risks. Once heavy metals enter the human body, they can inhibit enzyme activity, induce cytotoxicity, damage nerve tissues, and impair detoxification organs [221–223].

Low-silica zeolite A is an excellent material for addressing heavy metal contamination due to its high specific surface area and abundant cation-exchange sites. Several studies have explored its synthesis and application.

Cui et al. utilized a small amount of $TMA^+$ as an OSDA to synthesize low-silica zeolite A [224]. By adjusting the ratio of inorganic to organic structure-directing agents, they achieved a low Si/Al ratio, high crystallinity, reduced crystal size, and enhanced adsorption performance. Under optimal conditions—90 min of contact time, pH 5, 25 °C, and adsorbent dosage of 100 $mg \cdot g^{-1}$—the maximum adsorption capacities were 230 $mg \cdot g^{-1}$ for Cu(II) and 600 $mg \cdot g^{-1}$ for Pb(II).

Nseke et al. synthesized zeolite 4A from waste materials, including silicon sources and aluminum foil [225]. They optimized adsorption parameters for $Cu^{2+}$, $Zn^{2+}$, and $Cd^{2+}$, achieving capacities of 99.9 $mg \cdot g^{-1}$, 82.1 $mg \cdot g^{-1}$, and 103 $mg \cdot g^{-1}$, respectively. Key conditions included a zeolite dosage of 12 $g \cdot L^{-1}$, pH 6, a contact time of 1–3 h, and a temperature of 25–27.5 °C.

Mubarak et al. synthesized zeolite 4A from kaolin and modified it with $TiO_2$ [226]. The $TiO_2$@Zeolite-4A exhibited faster adsorption kinetics and higher removal efficiency for Fe(III) and Mn(II) at lower pH levels compared to unmodified zeolite.

Ghasemi et al. used microwave-assisted methods to prepare zeolite 4A for $Ni^{2+}$ removal [227]. The removal efficiency exceeded 99% under optimized conditions, with adsorption following the Langmuir isotherm model. The maximum capacity increased from 94.3 $mg \cdot g^{-1}$ at 298 K to 185.2 $mg \cdot g^{-1}$ at 333 K.

Meng et al. synthesized zeolite A from halloysite and evaluated its selectivity for heavy metal ions [189]. The material showed the highest selectivity for $Pb^{2+}$ and $Ag^+$, with capacities of 227.7 $mg \cdot g^{-1}$ and 123.0 $mg \cdot g^{-1}$, respectively. The selectivity order was $Ag^+ \sim Pb^{2+} > Cr^{3+} \sim Cu^{2+} \sim Zn^{2+} > Mn^{2+} \sim Ni^{2+} \sim Fe^{3+}$.

Rentsennorov et al. synthesized zeolite A from fly ash and reported an adsorption capacity of 35.8 $mg \cdot g^{-1}$ for Cr(III) [228]. The material reached equilibrium within 30 min, achieving 97% removal efficiency for a 10 mg/L Cr(III) solution. Xiao et al. synthesized zeolite A from CFA for Cr(VI) removal, reporting a lower capacity of 8.7 $mg \cdot g^{-1}$ [229]. To enhance Cr(VI) adsorption, Guan et al. modified zeolite 4A with water-soluble chitosan quaternary ammonium salt (HACC), achieving a capacity of 16.9 $mg \cdot g^{-1}$ [230].

Li et al. developed an environmentally friendly method for Hg(II) removal using NaA zeolite synthesized from CFA [231]. $Zn^{2+}$ and $S^{2-}$ ions were introduced into the zeolite channels via ion exchange to form ZnS nanoclusters. During $Hg^{2+}$ removal, $Hg^{2+}$ formed HgS compounds by exchanging with $Zn^{2+}$ in the ZnS-zeolite structure. This process prevented $Zn^{2+}$ leaching and secondary pollution. The ZnS-zeolite NaA composite exhibited an impressive $Hg^{2+}$ adsorption capacity of 553.2 $mg \cdot g^{-1}$ and maintained over 99.9% removal efficiency in the presence of $Pb^{2+}$, $Cd^{2+}$, and $Cu^{2+}$, with only a 2% reduction in efficiency after five cycles, demonstrating its strong potential for practical applications.

### *3.2. Removal of Radionuclide Cations*

Radionuclide cations such as $^{60}Co^{2+}$, $^{90}Sr^{2+}$, and $^{137}Cs^{+}$, are commonly found in wastewater generated from smelting, petrochemical processing, nuclear operations, and mineral mining. The Fukushima nuclear accident heightened concerns about safely treating nuclear fission products, particularly $^{137}Cs$ and $^{90}Sr$. Similar to other metal cations, these radionuclides can be effectively removed using zeolite A via ion exchange. In laboratory studies, non-radioactive cations are often used as proxies to simulate the adsorption behavior of radioactive counterparts.

Fang et al. compared the removal efficiencies of $^{137}Cs^{+}$, $^{90}Sr^{2+}$, and $^{60}Co^{2+}$ using zeolite 4A, natural zeolite, and vermiculite in laundry wastewater containing organic materials and suspended solids [232]. Zeolite 4A achieved the highest removal efficiencies, exceeding 90% for all three radionuclides under neutral conditions at room temperature and surpassing 98.7% under alkaline conditions.

Murukutti et al. synthesized zeolite A from CFA and evaluated its adsorption capacities for $^{137}Cs^{+}$ and $^{90}Sr^{2+}$ [233]. The adsorption capacities were 95.7 $mg \cdot g^{-1}$ for $^{137}Cs^{+}$ and 54.1 $mg \cdot g^{-1}$ for $^{90}Sr^{2+}$.

Lee et al. investigated the removal of $^{137}Cs$ using zeolite A [234]. Synchrotron X-ray diffraction studies revealed that as ion exchange progressed, $Cs^{+}$ ions shifted to occupy the centers of eight-membered rings (8MRs). **RHO** zeolite, which contains more 8MRs than zeolite A, exhibited superior adsorption performance for $Cs^{+}$, confirming the role of 8MRs in enhancing selectivity.

Wang et al. scaled up the synthesis of high-quality zeolite A (SFCC-A) from spent fluid catalytic cracking (FCC) catalysts to a 100 L batch [33]. SFCC-A exhibited an adsorption capacity of 180.5 $mg \cdot g^{-1}$ for $Co^{2+}$ and achieved over 99% removal efficiency at a pH range of 4-8 and a solid-to-liquid ratio of 1/1000. Its performance was comparable to that of commercial zeolite A, highlighting its potential for industrial applications.

Hao et al. studied the removal of $^{90}Sr^{2+}$ using NaA zeolite [235]. Adsorption capacity reached 294.1 $mg \cdot g^{-1}$ under optimized conditions, with a distribution coefficient $K_d$ of 421.56 $\pm$ 13.39 $L \cdot g^{-1}$. In radioactive wastewater containing high concentrations of $NaNO_3$ and $NH_4NO_3$, NaA zeolite maintained stable performance, reducing radioactive concentrations of 0.62 $\pm$ 0.12 $Bq \cdot L^{-1}$, near regulatory limits for drinking water. Structural Rietveld refinements showed that $Sr^{2+}$ occupied the center of the single six-membered rings (s6rs), while density functional theory (DFT) calculations confirmed high selectivity for $^{90}Sr^{2+}$ in eight-membered rings (s8rs). In related work, Wang et al. synthesized zeolite A from lithium slag, achieving a high adsorption capacity of 246.9 $mg \cdot g^{-1}$ for $Sr^{2+}$ with equilibrium reached within 5 min [32]. The material demonstrated effective performance across a wide pH range (4–13), confirming its potential for radioactive wastewater treatment.

Dahake et al. developed polyamidoxime-modified zeolite A for uranium adsorption [236]. The modified zeolite achieved a 98% removal efficiency for $[UO_2]^{2+}$, with an adsorption capacity of 4.6 mg $U \cdot g^{-1}$. Even in the presence of competitive ions such as

Cr, Cd, Co, Pb, and Mn, or after eight adsorption cycles, the removal efficiency remained above 90%.

### *3.3. Water Softening*

$Ca^{2+}$ and $Mg^{2+}$ ions are the primary contributors to water hardness. Hard water causes scaling in machines, boilers, and pipelines. It has also been linked to health issues, including cardiovascular disease, kidney stones, and certain cancers. Moreover, hard water reduces soap efficiency, increasing detergent consumption [237,238].

Kusrini et al. evaluated acid-activated zeolite A, synthesized from kaolin, for water softening [239]. At an initial concentration of 110 ppm and a solution volume of 20 mL, 1 g of zeolite A removed 96.0% of $Ca^{2+}$. Increasing the dosage to 2 g improved $Mg^{2+}$ removal efficiency to 94.9%.

Manna et al. synthesized zeolite A from CFA and red mud, achieving adsorption capacities of 184.6 $mg \cdot g^{-1}$ for $Ca^{2+}$ within 15 min and 253.9 $mg \cdot g^{-1}$ for $Mg^{2+}$ after 5 h [240]. Similarly, El-Nahas et al. produced low-cost zeolite A from waste silica gel and aluminum. Their zeolites removed over 90% of total hardness (>1000 ppm) within 30 min [241].

Xue et al. developed meso-zeolite A with intracrystalline mesopores (~3 nm diameter) [242]. These mesopores significantly reduced the activation energy for ion exchange, accelerating $Mg^{2+}$ diffusion. The hydrated $Mg^{2+}$ diffusion in meso-zeolite A was 17.5 times higher than in conventional zeolite A at 273 K.

Painer et al. synthesized zeolite A from perlite and tested it for water softening [243]. Their zeolite removed 99.8% of $Ca^{2+}$ and 93.4% of $Mg^{2+}$ from tap water, outperforming both **SOD** zeolite and perlite powder. These findings underscore the potential of zeolite A for water softening applications.

### *3.4. Removal of Ammonia-Nitrogen*

Ammonia-nitrogen, a non-metallic cationic pollutant, is commonly found in freshwater systems due to agricultural fertilizers and domestic sewage [244]. Elevated levels contribute to eutrophication, oxygen depletion, and toxicity to aquatic life [245]. Additionally, ammonia-nitrogen can corrode metals and pose indirect health risks when converted by nitrifying bacteria into nitrite and nitrate, which are harmful in drinking water [246].

Numerous studies have demonstrated the potential of zeolite A (**LTA**) for ammonia-nitrogen removal. Wang et al. synthesized zeolite A from foundry dust, achieving an adsorption capacity of 37.8 $mg \cdot g^{-1}$, which decreased to 28.6 $mg \cdot g^{-1}$ after four regeneration cycles [198]. Ren et al. used CFA to produce zeolite A, reporting an $NH_4^+$ adsorption capacity of 2.322 $mmol \cdot g^{-1}$ (41.8 $mg \cdot g^{-1}$) [247]. Similarly, Jiang et al. synthesized zeolite A from CFA with an $NH_4^+$ adsorption capacity of 41.2 $mg \cdot g^{-1}$ [248]. In both studies, the adsorption process followed pseudo-second-order kinetics and the Langmuir model. Zhao et al. synthesized zeolite NaA from halloysite, achieving an $NH_4^+$ adsorption capacity of 44.3 $mg \cdot g^{-1}$ with excellent regeneration and reusability [190]. Wu et al. produced zeolite 4A from opal waste rock, which exhibited a high $NH_4^+$ adsorption capacity of 53.1 $mg \cdot g^{-1}$ [151]. The adsorption isotherm followed the Freundlich model ($R^2 > 0.99$), suggesting multi-layer adsorption was feasible for $NH_4^+$ removal.

### *3.5. Removal of Inorganic Anion Pollutants*

Inorganic anions generally exhibit low adsorption efficiency on zeolite frameworks due to charge repulsion between the anions and negatively charged zeolite frameworks. To address this, researchers have modified zeolite A or developed composites to enhance anion removal from water.

For fluoride ($F^-$) removal, Wang et al. synthesized zeolite A from coal gangue, achieving a modest adsorption capacity of 4.7 $mg \cdot g^{-1}$ [249]. In contrast, Naskar synthesized

zeolite A from rice husk ash, modified it with colloidal hydrated alumina, and achieved an $F^-$ adsorption capacity of 104.2 $mg \cdot g^{-1}$, with recyclability up to three cycles [250]. Chakraborty et al. developed a zeolite A-MgO composite, which exhibited a similar $F^-$ adsorption capacity of 107.6 $mg \cdot g^{-1}$ and maintained performance for five cycles [251]. The adsorption process in these studies adhered to pseudo-second-order kinetics and the Langmuir model, indicating a monolayer, chemically driven adsorption mechanism.

Phosphate removal has also been investigated extensively. Kugbe et al. used a zeolite A-goethite nanocomposite to achieve a phosphate adsorption capacity of 500 $\mu mol \cdot g^{-1}$, outperforming the individual components [252]. Guan et al. functionalized zeolite 4A with tetraethylenepentamine, achieving an endothermic adsorption process with a maximum capacity of 28 $mg \cdot g^{-1}$ at 25 °C, following the Langmuir model [253]. Song et al. reported a La-containing magnetic NaA zeolite synthesized from coal gangue, which achieved a phosphate adsorption capacity of 44.6 $mg \cdot g^{-1}$, nine times higher than the precursor zeolite [253].

Arsenic removal has focused on As(III) and As(V) species, which exist as oxygen-containing anions in water. Pillewan et al. demonstrated the use of Cu-exchanged zeolite A for As(III) and As(V) removal, achieving adsorption capacities of 1.4 $mg \cdot g^{-1}$ for As(III) and 1.48 $mg \cdot g^{-1}$ for As(V) [254]. Abukhadra et al. developed a chitosan/zeolite A hybrid structure with an As(V) adsorption capacity of 125 $mg \cdot g^{-1}$. The adsorption behavior followed pseudo-second-order kinetics and the Freundlich isotherm models, indicating multi-layer adsorption driven by chemical interactions [255].

Other studies have explored the removal of additional anions. Ashraf et al. evaluated a cellulose fibers/zeolite A nanocomposite for selenium species removal, achieving adsorption capacities of 163 $mg \cdot g^{-1}$ for selenite, 212.4 $mg \cdot g^{-1}$ for selenite, and 109.3 $mg \cdot g^{-1}$ for selenomethionine [256]. The adsorption followed pseudo-first-order kinetics and the Langmuir model, indicating homogenous, monolayer adsorption.

### *3.6. Removal of Organic Pollutants*

Zeolite A has been extensively studied for removing organic pollutants, including dyes and pharmaceuticals. However, the large size of many organic molecules often prevents their penetration into the zeolite channels, limiting adsorption to the surface. To address this limitation, researchers have modified zeolite A to enhance its adsorption capacity for organic pollutant removal.

Haghjoo et al. synthesized zeolite A from CFA and modified it with hexadecyltrimethylammonium chloride (HDTMAC) [257]. The modified zeolite exhibited a glyphosate pesticide adsorption capacity of 769.2 $mg \cdot g^{-1}$ and a removal efficiency of 98.9%, demonstrating its potential for sewage purification.

Djioko et al. synthesized zeolite A from kaolin for ciprofloxacin removal, achieving an adsorption capacity of 87.7 $mg \cdot g^{-1}$ [258]. Using 20 mg of adsorbent in a 60 ppm ciprofloxacin solution, the removal efficiency reached 91.8% at 25 °C. Even after seven cycles, the removal efficiency remained high at 85.7%. The adsorption process followed pseudo-second-order kinetic and the Langmuir model, indicating a monolayer chemical adsorption mechanism.

Mostafa et al. prepared a chitosan/zeolite A (CS/ZA) composite to evaluate its performance against organophosphorus pesticides, including acephate, omthosate, and methyl parathion [259]. The adsorption capacities were 650.7 $mg \cdot g^{-1}$ for acephate, 506.5 $mg \cdot g^{-1}$ for omthosate, and 560.8 $mg \cdot g^{-1}$ for methyl parathion. In fixed-bed column systems (6 cm) with a flow rate of 5 $mL \cdot min^{-1}$ and pH 8, removal efficiencies were 78%, 57.6%, and 74.3%, respectively. Unlike most zeolite adsorbents, the adsorption followed a pseudo-first-order kinetic model, suggesting physical adsorption as the dominant mechanism.

Modified zeolite A has also been explored for dye removal. Muniandy et al. used NaOH-modified 3A zeolite to remove malachite green and methyl violet dyes, achieving adsorption capacities of 136 $mg \cdot g^{-1}$ and 186 $mg \cdot g^{-1}$, respectively [260]. Xu et al. synthesized zeolite A from CFA and achieved a maximum adsorption capacity of 40.6 $mg \cdot g^{-1}$ for acid fuchsin [261].

Nyankson et al. developed a zeolite A/$Fe_3O_4$ nanocomposite for methylene blue removal, achieving a Langmuir adsorption capacity of 2.6 $mg \cdot g^{-1}$ at 25 °C and a maximum adsorption efficiency of 97.5% [262]. After regeneration, the efficiency at pH 7 decreased slightly to 82.6%. Similarly, Elfeky et al. demonstrated that ZnO-modified zeolite A enhanced methylene blue removal efficiency from 67.8% to 94.8% [263].

Khalaf et al. investigated zeolite A modified with hexadecyltrimethylammonium bromide for Congo red removal [264]. Batch experiments showed a maximum removal efficiency of 99.2% after 90 min, with an adsorption capacity of 21.1 $mg \cdot g^{-1}$.

**Table 1.** Adsorption performance towards hazardous substances by zeolite A and zeolite A-based composites.

| Raw Material | Adsorbents | Pollutant | Adsorption Capacity | Removal Efficiency | Kinetics | Adsorption Isotherm | Ref. |
|---|---|---|---|---|---|---|---|
| Lithium slag | Zeolite A | Sr(II) | 246.9 $mg \cdot g^{-1}$ | 99.9% | pseudo-second-order | Langmuir | [32] |
| PCR * | Zeolite A | Sr(II) | 294.1 $mg \cdot g^{-1}$ | >99% | pseudo-second-order | Langmuir | [235] |
| PCR | Zeolite A | Sr(II) | 204.3 $mg \cdot g^{-1}$ | > 80% | pseudo-second-order | - | [265] |
| PCR | Zeolite A | Sr(II) | 5.4 $meq \cdot g^{-1}$ | 83% | - | - | [266] |
| Kaolinite and red mud | Magnetic zeolite A | Sr(II) | 172 $mg \cdot g^{-1}$ | 96.4% | pseudo-second-order | Langmuir | [267] |
| PCR | magnetic zeolite A | Cs(I)<br>Sr(II) | 229.3 $mg \cdot g^{-1}$<br>89.0 $mg \cdot g^{-1}$ | 81.4%<br>95.2% | pseudo-second-order | Langmuir | [268] |
| Metakaolin | Zeolite A | Sr(II)<br>Co(II) | 167.5 $mg \cdot g^{-1}$<br>118.5 $mg \cdot g^{-1}$ | - | pseudo-second-order | Langmuir | [269] |
| Halloysite | Zeolite A | Pb(II)<br>Ag(I) | 227.7 $mg \cdot g^{-1}$<br>123.0 $mg \cdot g^{-1}$ | 100% | - | - | [189] |
| PCR | Zeolite A | Cu(II)<br>Pb(II) | 230 $mg \cdot g^{-1}$<br>600 $mg \cdot g^{-1}$ | - | pseudo-second-order | Langmuir | [224] |
| Bagasse ash | Zeolite A | Cu(II)<br>Pb(II) | 63.2 $mg \cdot g^{-1}$<br>187.2 $mg \cdot g^{-1}$ | 40.2%<br>37.5% | - | - | [136] |
| Metakaolin | Magnetic zeolite NaA | Cu(II)<br>Pb(II) | 2.3mmol $\cdot g^{-1}$<br>2.3mmol $\cdot g^{-1}$ | >95%<br>>95% | - | - | [270] |
| Wheat husk | NaCl-modified **LTA** | Pb(II) | 321.8 $mg \cdot g^{-1}$ | - | - | - | [138] |
| BFA and CFA | ZBG<br>ZCF | Pb(II) | 625 $mg \cdot g^{-1}$<br>556 $mg \cdot g^{-1}$ | 100% | pseudo-second-order | Langmuir | [271] |
| CFA | Zeolite A | Pb(II) | 714.3 $mg \cdot g^{-1}$ | - | first-order | Langmuir | [272] |
| Metakaolin | Zeolite A | Pb(II) | 880 $mg \cdot g^{-1}$ | 74.5% | pseudo-second-order | Langmuir | [273] |
| Metakaolin | Zeolite A | Pb(II) | 529.7 $mg \cdot g^{-1}$ | >99% | pseudo-second-order | Langmuir | [274] |
| Lithium leach residue | Zeolite A | Pb(II)<br>Cd(II) | 487.8 $mg \cdot g^{-1}$<br>193.8 $mg \cdot g^{-1}$ | 100%<br>96.9% | pseudo-second-order | Langmuir | [275] |
| Rare earth tailings | Zeolite A | Cd(II)<br>Cu(II)<br>$NH_4^+$<br>P(V)<br>$F^-$ | 247.3 $mg \cdot g^{-1}$<br>137.1 $mg \cdot g^{-1}$<br>35 $mg \cdot g^{-1}$<br>13.8 $mg \cdot g^{-1}$<br>5.9 $mg \cdot g^{-1}$ | 99.6%<br>98.2%<br>70.0%<br>38.2%<br>15.4% | pseudo-second-order | Langmuir | [276] |
| PCR | Zeolite A | Pb(II)<br>Cu(II)<br>Cr(III)<br>Zn(II)<br>Co(II) | 400 $mg \cdot g^{-1}$<br>396 $mg \cdot g^{-1}$<br>391 $mg \cdot g^{-1}$<br>385 $mg \cdot g^{-1}$<br>393.5 $mg \cdot g^{-1}$ | 100%<br>99%<br>97%<br>96%<br>98% | pseudo-second-order | Langmuir | [277] |

**Table 1.** *Cont.*

| Raw Material | Adsorbents | Pollutant | Adsorption Capacity | Removal Efficiency | Kinetics | Adsorption Isotherm | Ref. |
|---|---|---|---|---|---|---|---|
| Perlite | Zeolite A | Eu(III)<br>Ce(III) | 6.0 $mg \cdot g^{-1}$<br>5.1 $mg \cdot g^{-1}$ | 99%<br>90% | - | Langmuir | [278] |
| Micrometersized **LTA** | Nano **LTA** | Cs(I) | 422 $mg \cdot g^{-1}$ | 45% | pseudo-first-order | Langmuir | [279] |
| Kaolin | Zeolite A lattices | Cs(I) | 106.3 $mg \cdot g^{-1}$ | - | pseudo-second-order | Freundlich | [280] |
| PCR | PAN–zeolite A | Cs(I)<br>Sr(II) | 214.1 $mg \cdot g^{-1}$<br>98.1 $mg \cdot g^{-1}$ | 90%<br>90% | pseudo-second-order | Langmuir and D–R | [281] |
| PCR | MWCNT @Zeolite A | Cs(I)<br>Sr(II) | 113 $mg \cdot g^{-1}$<br>107 $mg \cdot g^{-1}$ | - | pseudo-second-order | Langmuir | [282] |
| CFA | Zeolite A | Cs(I)<br>Sr(II) | 2.1 $mmol \cdot g^{-1}$<br>1.9 $mmol \cdot g^{-1}$ | - | pseudo-second-order | Langmuir | [283] |
| CFA | Zeolite A | Cr(III) | 35.8 $mg \cdot g^{-1}$ | 97% | - | Langmuir | [228] |
| Bauxite tailings | Zeolite A | Cr(III) | 85.1 $mg \cdot g^{-1}$ | 96.8% | - | - | [152] |
| CFA | Zeolite A | Cr(VI) | 8.7 $mg \cdot g^{-1}$ | - | - | - | [229] |
| PCR | 4A/HACC | Cr(VI) | 16.9 $mg \cdot g^{-1}$ | 92% | pseudo-second-order | Langmuir | [230] |
| Kaolin | Zeolite A | Cr(VI) | 9.7 $mg \cdot g^{-1}$ | 100% | - | - | [284] |
| PCR | Zeolite A/ $Fe_3O_4$/biochar | Cr(VI) | 46.9 $mg \cdot g^{-1}$ | 93.9% | pseudo-second-order | Langmuir | [285] |
| PCR | Zeolite A | Cr(III) | 70 $mg \cdot g^{-1}$ | - | pseudo-second-order | - | [197] |
| Kaolin | Zeolite A | Cr(III) | ~200 $mg \cdot g^{-1}$ | 99.8% | pseudo-second-order | - | [286] |
| PCR | m-ZPC | Cu(II)<br>Cr(III) | 3.9 $mg \cdot g^{-1}$<br>2.0 $mg \cdot g^{-1}$ | - | pseudo-second-order | Redlich–Peterson | [287] |
| Waste materials | Zeolite A | Cd(II)<br>Cu(II)<br>Zn(II) | 103 $mg \cdot g^{-1}$<br>99.9 $mg \cdot g^{-1}$<br>82.1 $mg \cdot g^{-1}$ | 96%<br>98~99.9%<br>80~85% | - | Freundlich and Langmuir | [225] |
| Woody biomass ash | Zeolite A | Cu(II)<br>Cd(II)<br>Pb(II) | 140.1 $mg \cdot g^{-1}$<br>223.5 $mg \cdot g^{-1}$<br>850.7 $mg \cdot g^{-1}$ | >99% | pseudo-second-order | Freundlich and Langmuir | [142] |
| CFA | Zeolite A | Ni(II)<br>Cd(II)<br>Pb(II) | 1.1 $mmol \cdot g^{-1}$<br>1.4 $mmol \cdot g^{-1}$<br>2.6 $mmol \cdot g^{-1}$ | - | pseudo-second order | Langmuir | [288] |
| PCR | Hierarchical **LTA** | Pb(II)<br>Cu(II)<br>Ni(II) | 510 $mg \cdot g^{-1}$<br>170 $mg \cdot g^{-1}$<br>100 $mg \cdot g^{-1}$ | - | pseudo-second-order | Langmuir | [25] |
| Red mud | Magnetic 4A-zeolite | Zn(II)<br>Cu(II)<br>Cd(II)<br>Ni(II)<br>Pb(II) | 45.4 $mg \cdot g^{-1}$<br>35.6 $mg \cdot g^{-1}$<br>56.5 $mg \cdot g^{-1}$<br>41.2 $mg \cdot g^{-1}$<br>100.0 $mg \cdot g^{-1}$ | - | pseudo-second-order | Langmuir | [194] |
| Red mud and coal gangue | Magnetic zeolite A | Cu(II)<br>Cd(II)<br>Pb(II) | 76.2 $mg \cdot g^{-1}$<br>92.2 $mg \cdot g^{-1}$<br>178.4 $mg \cdot g^{-1}$ | - | pseudo-first-order<br>pseudo-second-order<br>pseudo-second-order | Langmuir | [153] |
| Rice husk and waste aluminum cans | Geopolymer/ zeolite A | Co(II)<br>Cu(II)<br>Zn(II) | 127.2 $mg \cdot g^{-1}$<br>119.1 $mg \cdot g^{-1}$<br>121.8 $mg \cdot g^{-1}$ | - | pseudo-second order | Langmuir | [289] |
| Red mud and CGS | Magnetic zeolite A | Pb(II)<br>Cu(II) | 330.7 $mg \cdot g^{-1}$<br>142.7 $mg \cdot g^{-1}$ | 85% | pseudo-second-order<br>Elovich | Langmuir<br>Freundlich | [196] |
| Kaolin | $O_2$-plasma treatment Zeolite A | Cd(II) | 247.0 $mg \cdot g^{-1}$ | 71% | - | - | [290] |
| PCR | hierarchical **LTA** | Cd(II) | 324.3 $mg \cdot g^{-1}$ | 90% | pseudo-first-order | Langmuir | [291] |

**Table 1.** *Cont.*

| Raw Material | Adsorbents | Pollutant | Adsorption Capacity | Removal Efficiency | Kinetics | Adsorption Isotherm | Ref. |
|---|---|---|---|---|---|---|---|
| CFA | Zeolite A | Pb(II)<br>Cd(II) | 277.8 $mg \cdot g^{-1}$<br>87.7 $mg \cdot g^{-1}$ | - | pseudo-second order | Langmuir | [292] |
| PCR | Zeolite A | Zn(II) | 117.4 $mg \cdot g^{-1}$ | 79.6% | pseudo-second-order | Langmuir | [293] |
| PCR | Zeolite A | Zn(II)<br>Cd(II) | 4.0 $mmol \cdot g^{-1}$<br>2.0 $mmol \cdot g^{-1}$ | - | pseudo-second-order | Freundlich and D-R | [294] |
| PCR | Zeolite A | Cu(II) | 202.8 $mg \cdot g^{-1}$ | 70.3% | pseudo-first-order | Langmuir | [295] |
| PCR | $Fe_3O_4$@zeolite NaA | Cu(II) | 86.5 $mg \cdot g^{-1}$ | 86.5% | pseudo-second-order | Langmuir | [296] |
| PCR | magnetic zeolite A | Cu(II) | 170 $mg \cdot g^{-1}$ | 57% | - | Langmuir | [297] |
| PCR | Zeolite A | Cu(II) | 155.4 $mg \cdot g^{-1}$ | 93.3% | - | - | [298] |
| Coal gangue and aluminum ash | Zeolite A | Cu(II) | 75.0 $mg \cdot g^{-1}$ | 99% | pseudo-second-order | - | [121] |
| Coal gangue | ZMC<br>ZTC<br>ZAC | Cu(II) | 118.1 $mg \cdot g^{-1}$<br>116.7 $mg \cdot g^{-1}$<br>116.1 $mg \cdot g^{-1}$ | - | pseudo-second-order | Langmuir | [125] |
| PCR | Hierarchical **LTA** | Cu(II) | 341.5 $mg \cdot g^{-1}$ | - | pseudo-second-order | Freundlich | [299] |
| Low-grade bauxite | Zeolite A | Cd(II) | 161.3 $mg \cdot g^{-1}$ | 99.9% | pseudo-second-order | Langmuir and Freundlich | [300] |
| PCR | tGO-Zeo | Cd(II) | 196 $mg \cdot g^{-1}$ | - | - | Langmuir | [301] |
| Metakaolin | Zeolite A | Cu(II) | 698.1 $mg \cdot g^{-1}$ | - | pseudo-second-order | Langmuir | [302] |
| SFCC | Zeolite A | Co(II) | 180.5 $mg \cdot g^{-1}$ | 99.2% | pseudo-second-order | Langmuir | [33] |
| Agricultural waste | AAS<br>AWS | Co(II) | 235.2 $mg \cdot g^{-1}$<br>202.9 $mg \cdot g^{-1}$ | - | - | Freundlich | [303] |
| PCR | Zeolite A | Ni(II) | 94 $mg \cdot g^{-1}$ (25 °C)<br>132 $mg \cdot g^{-1}$ (45 °C)<br>185 $mg \cdot g^{-1}$ (60 °C) | 99.9% | pseudo-second-order | Langmuir | [227] |
| PCR | NaA/XG -alginate | Co(II)<br>Ni(II) | 43.9 $mg \cdot g^{-1}$<br>81.3 $mg \cdot g^{-1}$ | - | pseudo-second-order | Langmuir | [304] |
| Rice husk and waste aluminum cans | geopolymer/ zeolite A/ chitosan | Hg(II)<br>Pb(II) | 211.9 $mg \cdot g^{-1}$<br>269.5 $mg \cdot g^{-1}$ | - | pseudo-second-order | Langmuir | [305] |
| CFA | $NH_3$ modified zeolite 4A | Hg(II) | 53.6 $mg \cdot g^{-1}$ | 99.2% | pseudo-second-order | Langmuir | [306] |
| CFA | ZnS-zeolite NaA | Hg(II) | 553.2 $mg \cdot g^{-1}$ | >99.9% | pseudo-second-order | Langmuir and Freundlich | [231] |
| PCR | C@zeolite-ZnS | Hg(II) | 795.8 $mg \cdot g^{-1}$ | 99.9% | pseudo-second-order | Langmuir | [307] |
| Opal | Zeolite A | Hg(II) | 42.0 $mg \cdot g^{-1}$ | 70% | pseudo-second order | Langmuir | [308] |
| Commercial | Zeolite A | Th(IV) | 2.8 $meq \cdot g^{-1}$ | 50.4% | - | Langmuir | [309] |
| PCR | $Na_2SO_4$@ zeolite A with $MnO_2$ | $^{226}Ra$<br>$^{228}Ra$ | - | 78.7%<br>66.7% | - | - | [310] |
| PCR | Co-Zn-LTA | Tc(VII) | - | 88.3% | pseudo-second-order | - | [311] |
| PCR | Zeolite A | U(VI) | 0.95 $mg \cdot g^{-1}$ | 60-67% | pseudo-first-order | Langmuir | [312] |
| PCR | Zeolite A | U(VI) | 1.08 $mg \cdot g^{-1}$ | >96% | pseudo-first-order | Langmuir | [313] |
| Kaolin | TiO2@ Zeolites-4A | Fe(III)<br>Mn(II) | 150.1 $mg \cdot g^{-1}$<br>94.1 $mg \cdot g^{-1}$ | 94%<br>100% | pseudo-second-order | Freundlich and Langmuir | [226] |
| PCR | Agarose-Zeolite **LTA** | Al(III)<br>Mn(II)<br>Fe(III) | 15.8 $mg \cdot g^{-1}$<br>3.0 $mg \cdot g^{-1}$<br>19.2 $mg \cdot g^{-1}$ | 99.5%<br>95.6%<br>95.3% | - | - | [314] |

**Table 1.** *Cont.*

| Raw Material | Adsorbents | Pollutant | Adsorption Capacity | Removal Efficiency | Kinetics | Adsorption Isotherm | Ref. |
|---|---|---|---|---|---|---|---|
| Linz–Donawitz (LD) slag | Zeolite A | Fe(III) | 27.6 $mg \cdot g^{-1}$ | 99.9% | pseudo-second-order | Langmuir | [167] |
| PCR | Zeolite A | Mn(II) | 30 $mg \cdot g^{-1}$ (25 °C)<br>50 $mg \cdot g^{-1}$ (55 °C) | ~70% | - | Langmuir | [315] |
| Kaolinite | ZC<br>ZF | Mn(II) | 6.8 $mg \cdot g^{-1}$<br>7.2 $mg \cdot g^{-1}$ | 82.2%<br>99.9% | pseudo-second-order | Langmuir | [316] |
| Electrolytic manganese residue | Zeolite A | Mn(II)<br>Cd(II) | 119.5 $mg \cdot g^{-1}$<br>314.2 $mg \cdot g^{-1}$ | -<br>85.6% | pseudo-second-order | Langmuir | [184, 185] |
| PCR | Cu-LTA | As(III)<br>As(V) | 1.4 $mg \cdot g^{-1}$<br>1.5 $mg \cdot g^{-1}$ | >98% | pseudo-first-order | Langmuir | [254] |
| CFA | NZVI-5A | As(V) | 72.1 $mg \cdot g^{-1}$ | 84.0% | pseudo-second-order | Langmuir | [317] |
| PCR | Fe-HZ | As(V) | 5.1 $mg \cdot g^{-1}$ | - | pseudo-second-order | Langmuir | [318] |
| PCR | Zeolite 5A | As(V)<br>Pb(II) | 36.4 $mg \cdot g^{-1}$<br>46.7 $mg \cdot g^{-1}$ | >95% | Elovich model | Langmuir and Freundlich | [319] |
| CFA and red mud | Zeolite A | Ca(II)<br>Mg(II) | 184.6 $mg \cdot g^{-1}$<br>253.9 $mg \cdot g^{-1}$ | - | pseudo-second-order | - | [240] |
| Waste aluminum and silica gel | Zeolite A | Ca(II)<br>Mg(II) | 111.1 $mg \cdot g^{-1}$<br>for Ca(II) | 90% | pseudo-second-order<br>intraparticle diffusion | Freundlich and Temkin | [241] |
| PCR | Mesoporous **LTA** | Ca(II)<br>Mg(II) | 3.1 $mmol \cdot g^{-1}$<br>2.8 $mmol \cdot g^{-1}$ | - | pseudo-second-order | Dual-site Langmuir | [242] |
| Metakaolin | Zeolite A | Ca(II)<br>Mg(II) | 935 $mg \cdot g^{-1}$ | >94% | pseudo-second-order | Langmuir | [320] |
| Kaolin | Acid-activated zeolite A | Ca(II)<br>Mg(II) | - | 95.9%<br>94.9% | - | - | [239] |
| Perlite | Zeolite A | Ca(II)<br>Mg(II) | 2.7 $mmol \cdot g^{-1}$ | 99.8%<br>93.4% | - | - | [243] |
| PCR | Zeolite A | Cs(I)<br>Sr(II)<br>Ca(II)<br>Mg(II) | 1.6 $mmol \cdot g^{-1}$<br>5.5 $mmol \cdot g^{-1}$<br>4.8 $mmol \cdot g^{-1}$<br>4.2 $mmol \cdot g^{-1}$ | - | - | Dubinin–Radushkevich | [321] |
| CFA | Zeolite A | Ca(II) | 184 $mg \cdot g^{-1}$ | - | - | - | [322] |
| PCR | CTAB modified Zeolite A | Ca(II) | 129.3 $mg \cdot g^{-1}$ | 95.0% | pseudo-second-order | D–A and Langmuir | [323] |
| Bauxite tailings | Zeolite A | Ca(II) | 296 $mg \cdot g^{-1}$ | 38.4% | - | - | [324] |
| Coal gangue | Zeolite A | Ca(II) | 296.0 mg $CaCO3 \cdot g^{-1}$ | - | - | - | [122] |
| Coal gangue | Zeolite A | Ca(II) | 358 $mg \cdot g^{-1}$ | - | - | - | [44] |
| PCR | Polyamidoxime-modified zeolite A | U(VI) | 4.9 $mg \cdot g^{-1}$ | 98% | pseudo-second-order | Langmuir | [236] |
| PCR | Chitosan/ zeolite A | Cd(II)<br>As(V) | 170 $mg \cdot g^{-1}$<br>125 $mg \cdot g^{-1}$ | 100% | pseudo-first-order<br>pseudo-second-order | Freundlich | [255] |
| PCR | Nanomagnetite/ **LTA** | Dy(III) | 35 $mg \cdot g^{-1}$ | 100% | pseudo-second-order | Langmuir and Temkin | [325] |
| PCR | NaA membrane | $MoO_4^{2-}$ | - | 99.8% | - | - | [326] |
| PCR | Pt/**LTA** | Ba(II)<br>La(III) | 30.0 $mg \cdot g^{-1}$<br>14.8 $mg \cdot g^{-1}$ | 99.9%<br>99.9% | pseudo-second-order | Freundlich<br>Langmuir | [327] |
| PCR | Tetraethylene-pentamine-modified zeolite 4A | P(V) | 23 $mg \cdot g^{-1}$ | - | pseudo-second-order | Langmuir | [253] |

**Table 1.** *Cont.*

| Raw Material | Adsorbents | Pollutant | Adsorption Capacity | Removal Efficiency | Kinetics | Adsorption Isotherm | Ref. |
|---|---|---|---|---|---|---|---|
| PCR | Zeolite A–goethite | P(V) | 0.5 mmol·g$^{-1}$ | - | - | Langmuir | [252] |
| PCR | Fe-LTA | P(V) | 5.8 mg·g$^{-1}$ | 80% | pseudo-second-order | Langmuir | [328] |
| Coal gangue | LMZ | P(V) | 44.6 mg·g$^{-1}$ | 99.6% | - | - | [126] |
| Kaolin | $Co_3O_4$@ zeolite@ nano $SiO_2$ | P(V) | 344.8 mg·g$^{-1}$ | - | pseudo-first-order | Langmuir | [329] |
| PCR | CF/ZA | Se(VI)<br>Se(IV)<br>Se(Mt) | 163 mg·g$^{-1}$<br>212.4 mg·g$^{-1}$<br>109.3 mg·g$^{-1}$ | 100%<br>100%<br>79.7% | pseudo-first-order | Langmuir | [256] |
| Opal waste rock | Zeolite A | $NH_4^+$ | 53.1 mg·g$^{-1}$ | - | - | Freundlich | [151] |
| PCR | Zeolite A | $NH_4^+$ | 42.6 mg·g$^{-1}$ | - | pseudo-second-order | Langmuir | [330] |
| PCR | Zeolite A | $NH_4^+$ | 31.9 mg·g$^{-1}$ | - | - | Langmuir | [331] |
| PCR | $Fe_3O_4$/**LTA** | $NH_4^+$ | 10.5 mg·g$^{-1}$ | 84.0% | pseudo-second-order | Freundlich | [332] |
| Halloysite | Zeolite A | $NH_4^+$ | 44.3 mg·g$^{-1}$ | - | - | Langmuir and Freundlich | [190] |
| CFA | Zeolite A | $NH_4^+$ | 41.2 mg·g$^{-1}$ | >40% | pseudo-second-order | Langmuir | [248] |
| CFA | Zeolite A | $NH_4^+$ | 60.6 mg·g$^{-1}$ | 59.6% | - | Freundlich | [333] |
| CFA | Zeolite A | $NH_4^+$ | 2.3 mmol·g$^{-1}$ | - | - | - | [247] |
| Foundry dust | Zeolite A | $NH_4^+$ | 37.8 mg·g$^{-1}$ | 96.2% | pseudo-second-order | Langmuir | [198] |
| Halloysite | Chitosan/ zeolite A | $NH_4^+$ | 47.6 mg·g$^{-1}$ | - | - | Langmuir | [334] |
| Kaolin | Zeolite A | $NH_4^+$ | 122.0 mg·g$^{-1}$ | - | pseudo-second-order | Langmuir | [335] |
| PCR | Zeolite A | $NH_4^+$ | 73.0 mg·g$^{-1}$ | 95.8% | pseudo-second-order | Langmuir and Freundlich | [336] |
| PCR | Zeolite A | $NH_4^+$ | 94.2 mg N·g$^{-1}$ | 70.2% | pseudo-second-order | Freundlich | [337] |
| PCR | Zeolite A | $NH_4^+$ | 2.6 mmol·g$^{-1}$ | - | - | Langmuir | [338] |
| PCR | Zeolite A-MgO | $F^-$ | 107.6 mg·g$^{-1}$ | 72% | pseudo-second-order | Langmuir | [251] |
| Coal gangue | Zeolite A | $F^-$ | 4.7 mg·g$^{-1}$ | 94.8% | pseudo-second-order | - | [249] |
| Rice husk ash | Zeolite A | $F^-$ | 104.2 mg·g$^{-1}$ | 99% | pseudo-second-order | Langmuir | [250] |
| PCR | Zeolite A/$Fe_3O_4$ | Methylene blue | 2.6 mg·g$^{-1}$ | 97.5% | pseudo-second-order | Langmuir | [262] |
| Linz–Donawitz (LD) slag | Zeolite A | Methylene blue | 25.3 mg·g$^{-1}$ | 98.1% | pseudo-second-order | Langmuir | [168] |
| PCR | $Fe_3O_4$/ZA | Methylene blue | 40.4 mg·g$^{-1}$ | ~96.8% | pseudo-second-order | - | [339] |
| Kaolin | Zeolite A | Methylene blue | 44.4 mg·g$^{-1}$ | 99.4% | pseudo-second-order | Langmuir | [340] |
| CFA | Zeolite A | Methylene blue | 23.2 mg·g$^{-1}$ (25 °C)<br>43.8 mg·g$^{-1}$ (40 °C) | 82.9% | pseudo-second-order | Langmuir | [341] |
| PCR | $NaA_{mw}$ | Methylene blue | 64.8 mg·g$^{-1}$ | - | pseudo-first-order | Langmuir | [342] |
| PCR | MZ-A/RGO | Methylene blue<br>Pb(II) | 666.7 mg·g$^{-1}$<br>416.7 mg·g$^{-1}$ | 98.5%<br>93.9% | pseudo-second-order | Langmuir | [343] |
| PCR | 3A zeolite | Methyl violet | 136 mg·g$^{-1}$ | 60% | pseudo-first-order | Langmuir | [260] |
| PCR | 3A zeolite | Malachite green | 186 mg·g$^{-1}$ | 96% | pseudo-first-order | Langmuir | [260] |

**Table 1.** *Cont.*

| Raw Material | Adsorbents | Pollutant | Adsorption Capacity | Removal Efficiency | Kinetics | Adsorption Isotherm | Ref. |
|---|---|---|---|---|---|---|---|
| Waste aluminum cans | Zeolite A | Malachite green | 29.7 $mg \cdot g^{-1}$ | - | pseudo-second-order | Langmuir | [160] |
| PCR | HDTMABr modified **LTA** | Congo red | 21.1 $mg \cdot g^{-1}$ | 99.2% | pseudo-second-order | Temkin | [264] |
| CFA | Zeolite A | Acid fuchsin | 40.6 $mg \cdot g^{-1}$ | - | pseudo-first-order | Langmuir | [261] |
| CFA | Surfactant-modified-**LTA** | Glyphosate | 769.2 $mg \cdot g^{-1}$ | 98.9% | pseudo-second-order | Freundlich | [257] |
| PCR | Cu-LTA | Glyphosate | 112.7 $mg \cdot g^{-1}$ | - | pseudo-first-order and pseudo-second-order | Langmuir | [339] |
| Kaolin | Zeolite A | Ciprofloxacin | 87.7 $mg \cdot g^{-1}$ | 91.8% | pseudo-second-order | Langmuir | [258] |
| PCR | CS/ZA | AC<br>OM<br>MP | 650.7 $mg \cdot g^{-1}$<br>506.5 $mg \cdot g^{-1}$<br>560.8 $mg \cdot g^{-1}$ | 78%<br>57.6%<br>74.3% | pseudo-first-order | Langmuir | [259] |
| Clay | Zeolite A | Methylene blue<br>8-HQ | 77.1 $mg \cdot g^{-1}$<br>33.5 $mg \cdot g^{-1}$ | - | - | Freundlich | [344] |
| PCR | CS/ZA | Bezactive Orange 16 | 305.8 $mg \cdot g^{-1}$ | - | pseudo-second-order | Langmuir | [345] |
| Coal gangue | ZMC<br>ZTC<br>ZAC | Rh-B | 5.4 $mg \cdot g^{-1}$<br>13.1 $mg \cdot g^{-1}$<br>32.8 $mg \cdot g^{-1}$ | - | pseudo-second-order | Langmuir | [125] |
| PCR | GO/4A | Rh-B | 62.8 $mg \cdot g^{-1}$ | - | pseudo-second-order | Langmuir | [346] |
| CFA | Zeolite A | AR 66 | 416.7 $mg \cdot g^{-1}$ | 100% | pseudo-second-order | Freundlich | [347] |
| PCR | CTAB modified Zeolite A | Methyl orange | 22.4 $mg \cdot g^{-1}$ | 87.2% | - | Langmuir | [348] |

* PCR refers to pure chemical reagents.

## 4. Ion-Exchange Selectivity Order on Zeolite A

Studies on metal cation removal using zeolite A have demonstrated significant differences in ion-exchange selectivity. These differences manifest in the adsorption capacities of zeolite A for various cations, its preference in mixed cation systems, and the challenges of replacing one metal cation for another. These factors are influenced by the **LTA** framework's affinity for specific cations and the hydrated ion sizes.

For example, Finish et al. observed that zeolite 4A exhibited a much higher affinity for $Pb^{2+}$ and $Cr^{3+}$ compared to $Zn^{2+}$, $Cd^{2+}$, and $Ni^{2+}$ [349]. Similarly, Ibrahim et al. synthesized zeolite A from Egyptian kaolin and reported the selectivity order as $Pb^{2+} > Cd^{2+} > Cu^{2+} > Zn^{2+} > Ni^{2+}$ [350]. Meng et al. proposed a comparable order: $Ag^{+} \approx Pb^{2+} > Cr^{3+} \approx Cu^{2+} \approx Zn^{2+} > Mn^{2+} \approx Ni^{2+} \approx Fe^{3+}$ [189].

Hui et al. synthesized zeolite 4A from CFA and determined the selectivity order as $Cu^{2+} > Cr^{3+} > Zn^{2+} > Co^{2+} > Ni^{2+}$, based on adsorption capacity in $mg \cdot g^{-1}$ [351]. However, when normalized to molar adsorption ($mmol \cdot g^{-1}$), $Cr^{3+}$ exhibited a higher capacity than $Cu^{2+}$.

Hao et al. calculated the interaction energies of $Na^{+}$ within the *s8r* rings of the *lta* cage. They found that replacing all cations with $Na^{+}$ in the *s8r* was thermodynamically favorable (Table 2) [235]. This finding underscores the versatility of zeolite 4A for metal cation removal. Additional thermodynamic simulations and experimental studies reported a selectivity order of $Sr^{2+} > Ba^{2+} > Cd^{2+} > Ca^{2+} > Mg^{2+} > Cs^{+} > Na^{+}$ [321,352,353].

**Table 2.** Interaction energies (in eV) of $Na^+$ in the *s8r* of the *lta* cage exchanging with various cations. [235]. Copyright (2022) RSC.

| Adsorption Reaction | ΔE (eV) |
|---|---|
| LTA + $2H_2O$ + $NH_4^+ \cdot (H_2O)_4$ → LTA-$NH_4$ + $Na^+ \cdot (H_2O)_6$ | −0.65 |
| LTA + $K^+ \cdot (H_2O)_6$ → LTA-K + $Na^+ \cdot (H_2O)_6$ | −2.13 |
| LTA + $Cs^+ \cdot (H_2O)_6$ → LTA-Cs + $Na^+ \cdot (H_2O)_6$ | −0.11 |
| LTA + $6H_2O$ + $Mg^{2+} \cdot (H_2O)_6$ → LTA-Mg + $2Na^+ \cdot (H_2O)_6$ | −1.94 |
| LTA + $6H_2O$ + $Ca^{2+} \cdot (H_2O)_6$ → LTA-Ca + $2Na^+ \cdot (H_2O)_6$ | −6.17 |
| LTA + $6H_2O$ + $Sr^{2+} \cdot (H_2O)_6$ → LTA-Sr + $2Na^+ \cdot (H_2O)_6$ | −8.17 |

Integrating findings from multiple studies, the overall selectivity order for cations on zeolite A is as follows: $Ag^+ \approx Pb^{2+} > Sr^{2+} > Ba^{2+} > Cr^{3+} > Cd^{2+} > Cu^{2+} > Zn^{2+} > Co^{2+} > Ni^{2+} \approx Mn^{2+} \approx Fe^{3+} > Ca^{2+} > K^+ > Mg^{2+} > NH_4^+ > Cs^+ > Na^+$. Notably, aside from $Pb^{2+}$, zeolite A's affinity for most divalent cations is relatively similar, a subject of ongoing debate among researchers [354,355]. In practical applications, especially in multi-component systems, the separation efficiency for divalent cations may not always be distinct. However, the selectivity for monovalent ions—except $Ag^+$—is significantly lower. This indicates that divalent cations, such as $Cu^{2+}$, $Mn^{2+}$, and $Co^{2+}$, can be effectively separated from monovalent ions. Furthermore, the low selectivity for $Na^+$ enhances the suitability of zeolite A as an adsorbent for removing diverse metal cation pollutants.

## 5. Conclusions and Prospects

Adsorption methods are widely favored in water pollution treatment due to their simplicity, eco-friendliness, and low operation costs. Zeolite A has emerged as a highly effective material, offering broad adsorption capabilities for various pollutants.

This review has summarized recent advancements in the synthesis of **LTA** zeolites, with a focus on producing zeolite A with a low Si/Al ratio from natural materials and industrial solid wastes, without relying on OSDAs. The low Si/Al ratio increases the number of ion-exchange sites, thereby enhancing adsorption capacity. Furthermore, the development of cost-effective and environmentally friendly synthesis methods aligns with the growing demand for sustainable water treatment solutions.

We have also reviewed the current status of zeolite A and its derivatives in adsorbing various water pollutants, highlighting representative results as references for future research. For metal cation adsorption, we have outlined the selectivity order of different cations based on experimental data and findings from multiple studies, providing valuable insights into ion-exchange research.

Future research should focus on the development of low-cost, environmentally friendly zeolite A adsorbents derived from natural materials and industrial wastes, with a focus on enhancing their adsorption efficiency. The established ion-exchange selectivity order can be leveraged to optimize wastewater treatment processes, particularly for industrial and domestic effluents. This approach could also facilitate the selective recovery of valuable metal elements, contributing to circular economy practices and sustainable development.

The synthesis of zeolite A from solid waste has matured significantly, offering great potential for practical applications. Establishing on-site systems for synthesizing zeolite A directly at solid waste generation sites or near polluted water sources could further streamline the process. This integrated approach would convert solid waste into high-value zeolite A, which can then be immediately used to treat pollutants at the source. Such a system would eliminate the need to transport raw materials and adsorbents, reducing costs and improving overall sustainability.

**Author Contributions:** Conceptualization, B.W., J.P., and W.Y.; writing—original draft preparation, J.P.; writing—review and editing, W.Y.; visualization, S.L. (Simiao Liu), S.L. (Shanshan Liu), and J.P.; supervision, W.Y. All authors have read and agreed to the published version of the manuscript.

**Funding:** This research was funded by the National Key Research and Development Program of China (2022YFB3504000), the National Natural Science Foundation of China (22288101), the '111 Center' (B17020), the Innovation Platform for Academicians of Hainan Province, and the Specific Research Fund of the Innovation Platform for Academicians of Hainan Province (YSPTZX202321).

**Data Availability Statement:** No new data were created or analyzed in this study. Data sharing is not applicable to this article.

**Acknowledgments:** The authors would like to thank all reviewers for their constructive advice.

**Conflicts of Interest:** The authors declare no conflicts of interest.

## References

1. Opoku-Kwanowaa, Y.; Furaha, R.K.; Yan, L.; Wei, D. Effects of planting field on groundwater and surface water pollution in China. *Clean Soil Air Water* **2020**, *48*, 1900452. [CrossRef]
2. Meng, W. System engineering for water pollution control at the watershed level in China. *Front. Environ. Sci. Eng. China* **2009**, *3*, 443–452. [CrossRef]
3. Lin, L.; Yang, H.; Xu, X. Effects of water pollution on human health and disease heterogeneity: A review. *Front. Environ. Sci.* **2022**, *10*, 880246. [CrossRef]
4. Karaouzas, I.; Kapetanaki, N.; Mentzafou, A.; Kanellopoulos, T.D.; Skoulikidis, N. Heavy metal contamination status in Greek surface waters: A review with application and evaluation of pollution indices. *Chemosphere* **2021**, *263*, 128192. [CrossRef] [PubMed]
5. Hasan, M.K.; Shahriar, A.; Jim, K.U. Water pollution in Bangladesh and its impact on public health. *Heliyon* **2019**, *5*, e02145. [CrossRef]
6. Bellver-Domingo, Á.; Castellet-Viciano, L.; Hernández-Chover, V.; Hernández-Sancho, F. The quantification of non-action costs as an incentive to address water pollution problems. *Water* **2023**, *15*, 582. [CrossRef]
7. Babuji, P.; Thirumalaisamy, S.; Duraisamy, K.; Periyasamy, G. Human health risks due to exposure to water pollution: A review. *Water* **2023**, *15*, 2532. [CrossRef]
8. Zare, E.N.; Motahari, A.; Sillanpää, M. Nanoadsorbents based on conducting polymer nanocomposites with main focus on polyaniline and its derivatives for removal of heavy metal ions/dyes: A review. *Environ. Res.* **2018**, *162*, 173–195. [CrossRef] [PubMed]
9. Vardhan, K.H.; Kumar, P.S.; Panda, R.C. A review on heavy metal pollution, toxicity and remedial measures: Current trends and future perspectives. *J. Mol. Liq.* **2019**, *290*, 111197. [CrossRef]
10. Jiang, N.; Shang, R.; Heijman, S.G.J.; Rietveld, L.C. High-silica zeolites for adsorption of organic micro-pollutants in water treatment: A review. *Water Res.* **2018**, *144*, 145–161. [CrossRef] [PubMed]
11. Li, J.H.; Duan, H.B.; Shi, P.X. Heavy metal contamination of surface soil in electronic waste dismantling area: Site investigation and source-apportionment analysis. *Waste Manage. Res.* **2011**, *29*, 727–738.
12. Ejidike, I.P.; Onianwa, P.C. Assessment of trace metals concentration in tree barks as indicator of atmospheric pollution within Ibadan City, South-West, Nigeria. *J. Anal. Methods Chem.* **2015**, *2015*, 243601. [CrossRef] [PubMed]
13. Teh, C.Y.; Budiman, P.M.; Shak, K.P.Y.; Wu, T.Y. Recent advancement of coagulation–flocculation and its application in wastewater treatment. *Ind. Eng. Chem. Res.* **2016**, *55*, 4363–4389. [CrossRef]
14. Miklos, D.B.; Remy, C.; Jekel, M.; Linden, K.G.; Drewes, J.E.; Hübner, U. Evaluation of advanced oxidation processes for water and wastewater treatment—A critical review. *Water Res.* **2018**, *139*, 118–131. [CrossRef] [PubMed]
15. Hube, S.; Eskafi, M.; Hrafnkelsdóttir, K.F.; Bjarnadóttir, B.; Bjarnadóttir, M.Á.; Axelsdóttir, S.; Wu, B. Direct membrane filtration for wastewater treatment and resource recovery: A review. *Sci. Total Environ.* **2020**, *710*, 136375. [CrossRef] [PubMed]
16. Grandclément, C.; Seyssiecq, I.; Piram, A.; Wong-Wah-Chung, P.; Vanot, G.; Tiliacos, N.; Roche, N.; Doumenq, P. From the conventional biological wastewater treatment to hybrid processes, the evaluation of organic micropollutant removal: A review. *Water Res.* **2017**, *111*, 297–317. [CrossRef] [PubMed]
17. De Gisi, S.; Lofrano, G.; Grassi, M.; Notarnicola, M. Characteristics and adsorption capacities of low-cost sorbents for wastewater treatment: A review. *Sustainable Mater. Technol.* **2016**, *9*, 10–40. [CrossRef]
18. Chang, S.H. Utilization of green organic solvents in solvent extraction and liquid membrane for sustainable wastewater treatment and resource recovery—A review. *Environ. Sci. Pollut. Res.* **2020**, *27*, 32371–32388. [CrossRef] [PubMed]

19. Burakov, A.E.; Galunin, E.V.; Burakova, I.V.; Kucherova, A.E.; Agarwal, S.; Tkachev, A.G.; Gupta, V.K. Adsorption of heavy metals on conventional and nanostructured materials for wastewater treatment purposes: A review. *Ecotoxicol. Environ. Saf.* **2018**, *148*, 702–712. [CrossRef]
20. Huang, Y.; Wang, Y.; Liu, W.; Bu, L.; Qu, L.; Chu, K.; Guo, N.; Zhang, X.; Su, X.; Li, Y.; et al. Synthesis of LSX Using Seed-iteration Approach with High N2 Adsorption Capacity for Air Separation. *Chem. Res. Chin. Univ.* **2024**, *40*, 1192–1200. [CrossRef]
21. Jain, K.; Patel, A.S.; Pardhi, V.P.; Flora, S.J.S. Nanotechnology in wastewater management: A new paradigm towards wastewater treatment. *Molecules* **2021**, *26*, 1797. [CrossRef] [PubMed]
22. Kumar, S.; Ahlawat, W.; Bhanjana, G.; Heydarifard, S.; Nazhad, M.M.; Dilbaghi, N. Nanotechnology-based water treatment strategies. *J. Nanosci. Nanotechnol.* **2014**, *14*, 1838–1858. [CrossRef] [PubMed]
23. Rajasulochana, P.; Preethy, V. Comparison on efficiency of various techniques in treatment of waste and sewage water—A comprehensive review. *Resour.-Effic. Technol.* **2016**, *2*, 175–184.
24. Roshanfekr Rad, L.; Anbia, M. Zeolite-based composites for the adsorption of toxic matters from water: A review. *J. Environ. Chem. Eng.* **2021**, *9*, 106088. [CrossRef]
25. Hong, M.; Yu, L.; Wang, Y.; Zhang, J.; Chen, Z.; Dong, L.; Zan, Q.; Li, R. Heavy metal adsorption with zeolites: The role of hierarchical pore architecture. *Chem. Eng. J.* **2019**, *359*, 363–372. [CrossRef]
26. Ernst, S. Zeolites and catalysis. Synthesis, reactions and applications. Edited by Jiri Cejka, Avelino Corma and Stacey Zones. *Angew. Chem. Int. Ed.* **2011**, *50*, 5425–5426. [CrossRef]
27. Pérez-Pellitero, J.; Pirngruber, G.D. Industrial zeolite applications for gas adsorption and separation processes. *Struct. Bond.* **2020**, *184*, 195–225.
28. Vermeiren, W.; Gilson, J.-P. Impact of zeolites on the petroleum and petrochemical industry. *Top. Catal.* **2009**, *52*, 1131–1161. [CrossRef]
29. Wang, Y.; Han, J.; Jin, K.; Liu, S.; Li, Q.; Hou, P.; Liu, S.; Song, Q.; Wang, Z.; Tian, P.; et al. Fluoride-free synthesis of high-silica RHO zeolite for the highly selective synthesis of methylamine. *Inorg. Chem. Front.* **2024**, *11*, 5473–5483. [CrossRef]
30. Hao, W.; Yan, X.; Guo, X.; Wang, W.; Yan, T.; Zhang, J.-N.; Yan, W. Synthesis of a low-silica zeolite with exceptional selectivity for radioactive $^{137}Cs^{+}$. *Inorg. Chem. Front.* **2023**, *10*, 1894–1906. [CrossRef]
31. Nuić, I.; Trgo, M.; Vukojević Medvidović, N.; Ugrina, M. A mass transfer analysis of competitive binding of Pb, Cd, and Zn from binary systems onto a fixed zeolite bed. *Int. J. Environ. Res. Public Health* **2019**, *16*, 426. [CrossRef] [PubMed]
32. Wang, B.; Li, J.; Zhou, X.; Hao, W.; Zhang, S.; Lan, C.; Wang, X.; Wang, Z.; Xu, J.; Zhang, J.-N.; et al. Facile activation of lithium slag for the hydrothermal synthesis of zeolite A with commercial quality and high removal efficiency for the isotope of radioactive $^{90}Sr$. *Inorg. Chem. Front.* **2022**, *9*, 468–477. [CrossRef]
33. Wang, B.; Yan, Y.; Zhou, X.; Su, H.; Zhang, H.; Zhang, J.-N.; Xu, J.; Pan, Q.; Yan, W. Mild activation of spent fluid catalytic cracking (FCC) catalysts for the pilot synthesis of zeolite a with commercial quality and excellent $Co^{2+}$ removal ability. *Chem. Eng. J.* **2024**, *490*, 151733. [CrossRef]
34. Wang, Y.; Bai, P.; Jin, Z.; Li, Y.; Li, Y.; Shi, W.; Zhou, X.; Xu, J.; Yan, W.; Xu, R. Stellerite-seeded facile synthesis of zeolite heulandite with exceptional aqueous $Cd^{2+}$ capture performance. *Inorg. Chem. Front.* **2019**, *6*, 1785–1792. [CrossRef]
35. Dehmani, Y.; Ba Mohammed, B.; Oukhrib, R.; Dehbi, A.; Lamhasni, T.; Brahmi, Y.; El-Kordy, A.; Franco, D.S.P.; Georgin, J.; Lima, E.C.; et al. Adsorption of various inorganic and organic pollutants by natural and synthetic zeolites: A critical review. *Arabian J. Chem.* **2024**, *17*, 105474. [CrossRef]
36. Baerlocher, C.; McCusker, L.B. Database of Zeolite Structures. Available online: http://www.iza-structure.org/databases/ (accessed on 22 January 2025).
37. Collins, F.; Rozhkovskaya, A.; Outram, J.G.; Millar, G.J. A critical review of waste resources, synthesis, and applications for zeolite LTA. *Microporous Mesoporous Mater.* **2020**, *291*, 109667. [CrossRef]
38. Ikeda, T.; Kodaira, T.; Oh, T.; Nisawa, A. $K^{+}$ ion distribution in zeolite ZK-4's with various Si/Al ratios and the contribution of $K^{+}$ ions to K cluster formation. *Microporous Mesoporous Mater.* **2003**, *57*, 249–261. [CrossRef]
39. Kodaira, T.; Murakami, Y.; Inoue, S.-i. Magnetism based on the cluster orbital of K metal loaded ZK-4 zeolite. *Phys. B* **2005**, *359*, 1445–1447. [CrossRef]
40. Igarashi, M.; Kodaira, T.; Shimizu, T.; Goto, A.; Hashi, K. NMR property of arrayed K clusters in zeolite LTA with Si/Al=1.5. *J. Phys. Chem. Solids* **2006**, *67*, 1063–1066. [CrossRef]
41. Granato, M.A.; Vlugt, T.J.H.; Rodrigues, A.E. Study on hexane adsorption in zeolite ITQ-29 by molecular simulation. *Adsorption* **2008**, *14*, 763–770. [CrossRef]
42. Tiscornia, I.; Valencia, S.; Corma, A.; Téllez, C.; Coronas, J.; Santamaría, J. Preparation of ITQ-29 (Al-free zeolite A) membranes. *Microporous Mesoporous Mater.* **2008**, *110*, 303–309. [CrossRef]
43. Cheung, O.; Bacsik, Z.; Krokidas, P.; Mace, A.; Laaksonen, A.; Hedin, N. $K^{+}$ exchanged zeolite ZK-4 as a highly selective sorbent for $CO_2$. *Langmuir* **2014**, *30*, 9682–9690. [CrossRef]

44. Qian, T.; Li, J. Synthesis of Na-A zeolite from coal gangue with the in-situ crystallization technique. *Adv. Powder Technol.* **2015**, *26*, 98–104. [CrossRef]
45. El Bojaddayni, I.; Emin Küçük, M.; El Ouardi, Y.; Jilal, I.; El Barkany, S.; Moradi, K.; Repo, E.; Laatikainen, K.; Ouammou, A. A review on synthesis of zeolites from natural clay resources and waste ash: Recent approaches and progress. *Miner. Eng.* **2023**, *198*, 108086. [CrossRef]
46. Al-Jubouri, S.M.; Sabbar, H.A.; Waisi, B.I.; Lafta, H.A. Effect of synthesis parameters on the formation 4A zeolite crystals: Characterization analysis and heavy metals uptake performance study for water treatment. *Desalin. Water Treat.* **2019**, *165*, 290–300. [CrossRef]
47. Pham, T.-H.; Lee, B.-K.; Kim, J.; Lee, C.-H. Enhancement of $CO_2$ capture by using synthesized nano-zeolite. *J. Taiwan Inst. Chem. Eng.* **2016**, *64*, 220–226. [CrossRef]
48. Zahmakiran, M. Preparation and characterization of LTA-type zeolite framework dispersed ruthenium nanoparticles and their catalytic application in the hydrolytic dehydrogenation of ammonia–borane for efficient hydrogen generation. *Mater. Sci. Eng. B* **2012**, *177*, 606–613. [CrossRef]
49. Breck, D.W.; Eversole, W.G.; Milton, R.M. New synthetic crystalline zeolites. *J. Am. Chem. Soc.* **1956**, *78*, 2338–2339. [CrossRef]
50. Wakihara, T.; Sasaki, Y.; Kato, H.; Ikuhara, Y.; Okubo, T. Investigation of the surface structure of zeolite A. *Phys. Chem. Chem. Phys.* **2005**, *7*, 3416–3418. [CrossRef]
51. Newsam, J.M. The zeolite cage structure. *Science* **1986**, *231*, 1093–1099. [CrossRef] [PubMed]
52. Yang, J.; Cui, J.; Zhang, H.; Zhang, H.; Zhu, J. Kinetic and thermodynamic study of $Ag^+$, $Cu^{2+}$, and $Zn^{2+}$ ion adsorption on LTA for high-performance antibacterial coating. *Coatings* **2024**, *14*, 1524. [CrossRef]
53. Belviso, C.; Lettino, A.; Cavalcante, F. Influence of synthesis method on LTA time-dependent stability. *Molecules* **2018**, *23*, 2122. [CrossRef] [PubMed]
54. Madhu, J.; Madurai Ramakrishnan, V.; Santhanam, A.; Natarajan, M.; Palanisamy, B.; Velauthapillai, D.; Lan Chi, N.T.; Pugazhendhi, A. Comparison of three different structures of zeolites prepared by template-free hydrothermal method and its $CO_2$ adsorption properties. *Environ. Res.* **2022**, *214*, 113949. [CrossRef] [PubMed]
55. Tatlier, M.; Atalay-Oral, C.; Bayrak, A.; Maraş, T.; Erdem, A. Impact of ion exchange on zeolite hydrophilicity/hydrophobicity monitored by water capacity using thermal analysis. *Thermochim. Acta* **2022**, *713*, 179240. [CrossRef]
56. Anand, C.; Yamaguchi, Y.; Liu, Z.; Ibe, S.; Elangovan, S.P.; Ishii, T.; Ishikawa, T.; Endo, A.; Okubo, T.; Wakihara, T. Pioneering in situ recrystallization during bead milling: A top-down approach to prepare zeolite A nanocrystals. *Sci. Rep.* **2016**, *6*, 29210. [CrossRef] [PubMed]
57. Yanyan, J.; Bing, Z.; Wu, Z.; Bo, Z.; Hongbo, L.; Dongmei, W.; Ying, L. High-efficient synthesis of zeolite LTA via a wet-gel crystallization route. *Chem. Res. Chin. Univ.* **2017**, *33*, 520–524.
58. Palčić, A.; Sekovanić, L.; Subotić, B.; Bronić, J. Zeolite A synthesis under dynamic conditions, after hydrogel ageing. *Croat. Chem. Acta* **2012**, *85*, 297–301. [CrossRef]
59. Balkus, K.J.; Ly, K.T. The preparation and characterization of an X-type zeolite: An experiment in solid-state chemistry. *J. Chem. Educ.* **1991**, *68*, 875. [CrossRef]
60. Arafat, S.M.Y.; Reza, M.N.; Khan, G.M.A. Linde type-A zeolite synthesis and effect of crystallization on its surface acidity. *Indian J. Chem. Technol.* **2011**, *17*, 303–308.
61. Paprica, N.; Filipović, R.; Perušić, M.; Kostić, D.; Pantić, S.; Damjanović, V. Influence of the $SiO_2/Al_2O_3$ molar ratio on the specific properties of NaA zeolite. *Chem. Pap.* **2022**, *76*, 5421–5428. [CrossRef]
62. Wang, S.; Vaughan, J.; Xia, F.; Etschmann, B.; Brugger, J.; Brand, H.; Peng, H. Revealing the effect of anions on the formation and transformation of zeolite LTA in caustic solutions: An in situ synchrotron PXRD study. *Cryst. Growth Des.* **2023**, *23*, 3660–3670. [CrossRef]
63. Jafari, M.; Mohammadi, T.; Kazemimoghadam, M. Synthesis and characterization of ultrafine sub-micron Na-LTA zeolite particles prepared via hydrothermal template-free method. *Ceram. Int.* **2014**, *40*, 12075–12080. [CrossRef]
64. Huang, Y.; Li, M.; Shi, C.; Liu, Z.; Ren, B. Synthesis of ultra-small NaA zeolite nanocrystals at near room temperature. *J. Porous Mater.* **2023**, *30*, 1143–1147. [CrossRef]
65. Zhang, X.; Tong, D.; Jia, W.; Tang, D.; Li, X.; Yang, R. Studies on room-temperature synthesis of zeolite NaA. *Mater. Res. Bull.* **2014**, *52*, 96–102. [CrossRef]
66. Sun, X.; Wang, J.; Jiang, Y.; Maturura, E.; Wang, W.; Yang, R.; Xing, C.; Chen, J.; Tsubaki, N. Facile synthesis of zeolites under an atmospheric reflux system. *Microporous Mesoporous Mater.* **2022**, *331*, 111646. [CrossRef]
67. Chandrasekhar, S.; Pramada, P.N. Microwave assisted synthesis of zeolite A from metakaolin. *Microporous Mesoporous Mater.* **2008**, *108*, 152–161. [CrossRef]
68. Youssef, H.; Ibrahim, D.; Komarneni, S. Microwave-assisted versus conventional synthesis of zeolite A from metakaolinite. *Microporous Mesoporous Mater.* **2008**, *115*, 527–534. [CrossRef]

69. Andaç, Ö.; Tatlıer, M.; Sirkecioğlu, A.; Ece, I.; Erdem-Şenatalar, A. Effects of ultrasound on zeolite A synthesis. *Microporous Mesoporous Mater.* **2005**, *79*, 225–233. [CrossRef]
70. Sharma, P.; Yeo, J.-g.; Kim, D.K. Organic additive free synthesis of mesoporous naoncrystalline NaA zeolite using high concentration inorganic precursors. *J. Mater. Chem.* **2012**, *22*, 2838–2843. [CrossRef]
71. Fang, Y.; Hu, Y.; Liang, X.; Wang, S.; Zuo, S.; Gao, X.; Zhang, Z. Microwave hydrothermal synthesis and performance of NaA zeolite monolithic adsorbent with honeycomb ceramic matrix. *Microporous Mesoporous Mater.* **2018**, *259*, 116–122. [CrossRef]
72. Mintova, S.; Olson, N.; Valtchev, V.; Bein, T. Mechanism of zeolite A nanocrystal growth from colloids at room temperature. *Science* **1999**, *283*, 958–960. [CrossRef] [PubMed]
73. Yu, S.; Kwon, S.; Na, K. Synthesis of LTA zeolites with controlled crystal sizes by variation of synthetic parameters: Effect of $Na^+$ concentration, aging time, and hydrothermal conditions. *J. Sol-Gel Sci. Technol.* **2021**, *98*, 411–421. [CrossRef]
74. Bayati, B.; Babaluo, A.A.; Karimi, R. Hydrothermal synthesis of nanostructure NaA zeolite: The effect of synthesis parameters on zeolite seed size and crystallinity. *J. Eur. Ceram. Soc.* **2008**, *28*, 2653–2657. [CrossRef]
75. Anbia, M.; Koohsaryan, E.; Borhani, A. Novel hydrothermal synthesis of hierarchically-structured zeolite LTA microspheres. *Mater. Chem. Phys.* **2017**, *193*, 380–390. [CrossRef]
76. Feng, Y.C.; Meng, Y.; Li, F.X.; Lv, Z.P.; Xue, J.W. Synthesis of mesoporous LTA zeolites with large BET areas. *J. Porous Mater.* **2013**, *20*, 465–471. [CrossRef]
77. Nagase, T.; Miyakawa, M.; Nishioka, M. Template-free mesoporous LTA zeolite synthesized using microwave heating in the flow system. *Microporous Mesoporous Mater.* **2020**, *306*, 110375. [CrossRef]
78. Song, G.; Li, F.; Lv, Z.; Xue, J. Synthesis and characterization of a novel single-crystalline core–shell zeolite A. *Mater. Lett.* **2015**, *161*, 57–59. [CrossRef]
79. Wang, Y.; Ren, F.-f.; Pan, D.-h.; Ma, J.-h. A hierarchically micro-meso-macroporous zeolite CaA for methanol conversion to dimethyl ether. *Crystals* **2016**, *6*, 155. [CrossRef]
80. Chen, H.; Wydra, J.; Zhang, X.; Lee, P.-S.; Wang, Z.; Fan, W.; Tsapatsis, M. Hydrothermal synthesis of zeolites with three-dimensionally ordered mesoporous-imprinted structure. *J. Am. Chem. Soc.* **2011**, *133*, 12390–12393. [CrossRef]
81. Cho, K.; Cho, H.S.; de Ménorval, L.-C.; Ryoo, R. Generation of mesoporosity in LTA zeolites by organosilane surfactant for rapid molecular transport in catalytic application. *Chem. Mater.* **2009**, *21*, 5664–5673. [CrossRef]
82. Hasan, F.; Singh, R.; Li, G.; Zhao, D.; Webley, P.A. Direct synthesis of hierarchical LTA zeolite via a low crystallization and growth rate technique in presence of cetyltrimethylammonium bromide. *J. Colloid Interface Sci.* **2012**, *382*, 1–12. [CrossRef] [PubMed]
83. Hasan, F.; Singh, R.; Webley, P.A. Formation of LTA zeolite crystals with multi-hollow polycrystalline core–shell structure via aggregation–recrystallization route in presence of emulsion droplets. *Microporous Mesoporous Mater.* **2012**, *160*, 75–84. [CrossRef]
84. Bingre, R.; Louis, B.; Nguyen, P. An overview on zeolite shaping technology and solutions to overcome diffusion limitations. *Catalysts* **2018**, *8*, 163. [CrossRef]
85. Müller, P.; Russell, A.; Tomas, J. Influence of binder and moisture content on the strength of zeolite 4A granules. *Chem. Eng. Sci.* **2015**, *126*, 204–215. [CrossRef]
86. Yu, L.; Gong, J.; Zeng, C.; Zhang, L. Synthesis of monodisperse zeolite A/chitosan hybrid microspheres and binderless zeolite A microspheres. *Ind. Eng. Chem. Res.* **2012**, *51*, 2299–2308. [CrossRef]
87. Akhtar, F.; Andersson, L.; Ogunwumi, S.; Hedin, N.; Bergström, L. Structuring adsorbents and catalysts by processing of porous powders. *J. Eur. Ceram. Soc.* **2014**, *34*, 1643–1666. [CrossRef]
88. Liu, P.; Wu, Q.; Chen, Z.; Xiao, F.-S. Recent Advances in the Synthesis of Zeolites from Solid Wastes. *Chem. Res. Chin. Univ.* **2024**, *40*, 646–656. [CrossRef]
89. Tang, Y.; Wang, Q.; Yan, N.; Zhang, X.; Yang, M.; Tian, P.; Liu, Z. Highly Selective CO2 Separation on Na-exchanged DNL-6 Synthesized by Utilization of Spent Industrial Catalyst. *Chem. Res. Chin. Univ.* **2024**, *40*, 1171–1178. [CrossRef]
90. Han, X.; Xia, H.; Tu, W.; Wei, Y.; Xue, D.; Li, M.; Yan, W.; Zhang, J.-N.; Han, Y.-F. Zeolite-confined Fe-site Catalysts for the Hydrogenation of CO2 to Produce High-value Chemicals. *Chem. Res. Chin. Univ.* **2024**, *40*, 78–95. [CrossRef]
91. Bo, S.; Wang, T.; Lv, T.; Wu, H.; Feng, Z.; Miao, L.; Feng, Z.; Ren, L.; Meng, C. Rapid Synthesis of Boron-MWW Zeolite Through a Solvent-free Strategy. *Chem. Res. Chin. Univ.* **2024**, *40*, 1245–1255. [CrossRef]
92. Ahmaruzzaman, M. A review on the utilization of fly ash. *Prog. Energy Combust. Sci.* **2010**, *36*, 327–363. [CrossRef]
93. Hosseini Asl, S.M.; Javadian, H.; Khavarpour, M.; Belviso, C.; Taghavi, M.; Maghsudi, M. Porous adsorbents derived from coal fly ash as cost-effective and environmentally-friendly sources of aluminosilicate for sequestration of aqueous and gaseous pollutants: A review. *J. Cleaner Prod.* **2019**, *208*, 1131–1147. [CrossRef]
94. Kazemian, H.; Naghdali, Z.; Ghaffari Kashani, T.; Farhadi, F. Conversion of high silicon fly ash to Na-P1 zeolite: Alkaline fusion followed by hydrothermal crystallization. *Adv. Powder Technol.* **2010**, *21*, 279–283. [CrossRef]
95. Freitas, J.V.; Farinas, C.S. Sugarcane bagasse fly ash as a no-cost adsorbent for removal of phenolic inhibitors and improvement of biomass saccharification. *ACS Sustainable Chem. Eng.* **2017**, *5*, 11727–11736. [CrossRef]

96. Kumar, S.; Patil, C.B. Estimation of resource savings due to fly ash utilization in road construction. *Resour. Conserv. Recycl.* **2006**, *48*, 125–140. [CrossRef]
97. Guozhi, L.; Zhang, T.; Cheng, C.; Zhang, W.; Wang, L.; Wang, Y.; Zhang, Z. Zeolite a preparation from high alumina fly ash of china using alkali fusion and hydrothermal synthesis method. *Mater. Res. Express* **2019**, *6*, 065049. [CrossRef]
98. Liu, L.; Singh, R.; Xiao, P.; Webley, P.A.; Zhai, Y. Zeolite synthesis from waste fly ash and its application in $CO_2$ capture from flue gas streams. *Adsorption* **2011**, *17*, 795–800. [CrossRef]
99. Cao, J.; Wang, P.; Sun, Q. Green synthesis of magnetic zeolite LTA using NaOH activated fly ash. *Z. Anorg. Allg. Chem.* **2020**, *646*, 1666–1670. [CrossRef]
100. Fan, Y.; Huang, R.; Liu, Q.; Cao, Q.; Guo, R. Synthesis of zeolite A from fly ash and its application in the slow release of urea. *Waste Manage.* **2023**, *158*, 47–55. [CrossRef] [PubMed]
101. Yang, L.; Qian, X.; Yuan, P.; Bai, H.; Miki, T.; Men, F.; Li, H.; Nagasaka, T. Green synthesis of zeolite 4A using fly ash fused with synergism of NaOH and $Na_2CO_3$. *J. Cleaner Prod.* **2019**, *212*, 250–260. [CrossRef]
102. Nowak, P.; Muir, B.; Solińska, A.; Franus, M.; Bajda, T. Synthesis and characterization of zeolites produced from low-quality coal fly ash and wet flue gas desulphurization wastewater. *Materials* **2021**, *14*, 1558. [CrossRef] [PubMed]
103. Kunecki, P.; Panek, R.; Wdowin, M.; Franus, W. Synthesis of faujasite (FAU) and tschernichite (LTA) type zeolites as a potential direction of the development of lime Class C fly ash. *Int. J. Miner. Process.* **2017**, *166*, 69–78. [CrossRef]
104. Chareonpanich, M.; Jullaphan, O.; Tang, C. Bench-scale synthesis of zeolite A from subbituminous coal ashes with high crystalline silica content. *J. Cleaner Prod.* **2011**, *19*, 58–63. [CrossRef]
105. Hadi, A.A.; Malek, N.A.N.N.; Williams, C.D. Structural characterization and antibacterial activity of antibiotic streptomycin immobilized on zeolite synthesized from natural kaolinite. *Biointerface Res. Appl. Chem.* **2021**, *11*, 13573–13586.
106. Mgbemere, H.E.; Ekpe, I.C.; Lawal, G.; Ovri, H.; Chaudhary, A.-L. Preparation and characterization of zeolite type 4A using kaolin from ajebo, nigeria. *Pertanika J. Sci. Technol.* **2019**, *27*, 2427–2438.
107. Wang, P.; Sun, Q.; Zhang, Y.; Cao, J.; Li, X. Hydrothermal synthesis of Zeolite NaA from kaolin. *Funct. Mater. Lett.* **2019**, *12*, 1950075. [CrossRef]
108. Chandrasekhar, S. Influence of metakaolinization temperature on the formation of zeolite 4A from kaolin. *Clay Miner.* **1996**, *31*, 253–261. [CrossRef]
109. Holmes, S.M.; Alomair, A.A.; Kovo, A.S. The direct synthesis of pure zeolite-A using 'virgin' Kaolin. *RSC Adv.* **2012**, *2*, 11491–11494. [CrossRef]
110. Schwanke, A.J.; Silveira, D.R.; Saorin Puton, B.M.; Cansian, R.L.; Bernardo-Gusmão, K. Sustainable conversion of Brazilian Amazon kaolin mining waste to zinc-based Linde Type A zeolites with antibacterial activity. *J. Cleaner Prod.* **2022**, *338*, 130659. [CrossRef]
111. Wang, P.; Sun, Q. Synthesis and characterisation of zeolite LTA with sheet structure. *Micro Nano Lett.* **2020**, *15*, 433–436. [CrossRef]
112. Wang, J.-Q.; Huang, Y.-X.; Pan, Y.; Mi, J.-X. Hydrothermal synthesis of high purity zeolite A from natural kaolin without calcination. *Microporous Mesoporous Mater.* **2014**, *199*, 50–56. [CrossRef]
113. Tompsett, G.A.; Conner, W.C.; Yngvesson, K.S. Microwave synthesis of nanoporous materials. *ChemPhysChem* **2006**, *7*, 296–319. [CrossRef] [PubMed]
114. Oliveira, M.R.; Cecilia, J.A.; Ballesteros-Plata, D.; Barroso-Martín, I.; Núñez, P.; Infantes-Molina, A.; Rodríguez-Castellón, E. Microwave-assisted synthesis of zeolite A from metakaolinite for $CO_2$ adsorption. *Int. J. Mol. Sci.* **2023**, *24*, 14040. [CrossRef] [PubMed]
115. Chen, M. Eigenvalues, inequalities and ergodic theory. *Chin. Sci. Bull.* **2000**, *45*, 769–774. [CrossRef]
116. Yang, X.; Liu, Y.; Yan, C.; Chen, G. Solvent-free preparation of hierarchical 4A zeolite monoliths: Role of experimental conditions. *J. Cryst. Growth* **2019**, *528*, 125286. [CrossRef]
117. Si, J.; Guo, R.; Zhang, Y.; Ning, W.; Sun, Y.; Li, W.; Miao, S. Synthesis of Linde A-type zeolite from ball clay with incorporated ruthenium and application in hydrogenation catalysis. *Appl. Clay Sci.* **2023**, *239*, 106897. [CrossRef]
118. García, G.; Aguilar-Mamani, W.; Carabante, I.; Cabrera, S.; Hedlund, J.; Mouzon, J. Preparation of zeolite A with excellent optical properties from clay. *J. Alloys Compd.* **2015**, *619*, 771–777. [CrossRef]
119. Foroughi, M.; Salem, A.; Salem, S. Potential of fusion technique in production of mesoporous zeolite A powder from poor kaolin through modification by boehmite: Effect of clay mineralogy on particle morphology. *Adv. Powder Technol.* **2021**, *32*, 2423–2432. [CrossRef]
120. Wang, X.-M.; Zhao, B.; Zhang, C.-S.; Zhang, Q.-L. Paste-like self-flowing transportation backfilling technology based on coal gangue. *Min. Sci. Technol.* **2009**, *19*, 137–143. [CrossRef]
121. Wang, Q.; Xu, W.; Cai, J.; Yu, Q.; Min, J. Study on the synthesis of LTA-Type molecular sieves from coal gangue and aluminum ash and its adsorption properties towards $Cu^{2+}$. *Crystals* **2024**, *14*, 379. [CrossRef]
122. Liu, S.; Yan, S.; Li, Y.; Cao, J. Synthesis of zeolite A with high whiteness from coal gangue by two-step pretreatment method. *Asia-Pac. J. Chem. Eng.* **2022**, *17*, e2760. [CrossRef]

123. Kong, D.; Jiang, R. Preparation of NaA zeolite from high iron and quartz contents coal gangue by acid leaching—Alkali melting activation and hydrothermal synthesis. *Crystals* **2021**, *11*, 1198. [CrossRef]
124. Jin, Y.; Li, L.; Liu, Z.; Zhu, S.; Wang, D. Synthesis and characterization of low-cost zeolite NaA from coal gangue by hydrothermal method. *Adv. Powder Technol.* **2021**, *32*, 791–801. [CrossRef]
125. Li, H.; Zheng, F.; Wang, J.; Zhou, J.; Huang, X.; Chen, L.; Hu, P.; Gao, J.-m.; Zhen, Q.; Bashir, S.; et al. Facile preparation of zeolite-activated carbon composite from coal gangue with enhanced adsorption performance. *Chem. Eng. J.* **2020**, *390*, 124513. [CrossRef]
126. Song, L.; Li, J.; Zhang, Z.; Li, Z.; Hu, T.; Li, F.; Zhao, Y.; Peng, X. La-containing magnetic zeolite synthesized from gangue by ball-milling method. *Mater. Lett.* **2021**, *303*, 130542. [CrossRef]
127. Bohra, S.; Kundu, D.; Naskar, M.K. One-pot synthesis of NaA and NaP zeolite powders using agro-waste material and other low cost organic-free precursors. *Ceram. Int.* **2014**, *40*, 1229–1234. [CrossRef]
128. Pode, R. Potential applications of rice husk ash waste from rice husk biomass power plant. *Renew. Sustain. Energy Rev.* **2016**, *53*, 1468–1485. [CrossRef]
129. Schmitz, T.; Schneider, H.; Schwanke, A.J.; Tessaro, I.C.; Marcilio, N.R. LTA zeolite from rice husk ash: Influence of the silicon source. *Ind. Biotechnol.* **2022**, *18*, 191–196. [CrossRef]
130. Simanjuntak, W.; Pandiangan, K.D.; Sembiring, Z.; Simanjuntak, A.; Hadi, S. The effect of crystallization time on structure, microstructure, and catalytic activity of zeolite-A synthesized from rice husk silica and food-grade aluminum foil. *Biomass Bioenergy* **2021**, *148*, 106050. [CrossRef]
131. Yusof, A.M.; Nizam, N.A.; Rashid, N.A.A. Hydrothermal conversion of rice husk ash to faujasite-types and NaA-type of zeolites. *J. Porous Mater.* **2010**, *17*, 39–47. [CrossRef]
132. Madhu, J.; Santhanam, A.; Natarajan, M.; Velauthapillai, D. $CO_2$ adsorption performance of template free zeolite A and X synthesized from rice husk ash as silicon source. *RSC Adv.* **2022**, *12*, 23221–23239. [CrossRef] [PubMed]
133. Ghasemi, Z.; Younesi, H. Preparation of free-template nanometer-sized Na–A and –X zeolites from rice husk ash. *Waste Biomass Valorization* **2012**, *3*, 61–74. [CrossRef]
134. Tan, W.-C.; Yap, S.-Y.; Matsumoto, A.; Othman, R.; Yeoh, F.-Y. Synthesis and characterization of zeolites NaA and NaY from rice husk ash. *Adsorption* **2011**, *17*, 863–868. [CrossRef]
135. Nawog, M.A.; Muhid, M.N.M.; Malek, N.A.N.N.; Hamdan, H. Eco-friendly synthesis of nanozeolite NaA from rice husk ash and its efficiency in removing ammonium ions. *Key Eng. Mater.* **2014**, *594–595*, 168–172. [CrossRef]
136. Hameed, Y.N.-u.-A.; Alam, S.; Sultana, S.; Gul, S.; Naveed, A. Synthesis of zeolite-A from bagasse ash and removal of heavy metals from industrial effluents. *Adv. Cem. Res.* **2021**, *33*, 398–402.
137. Esmaeili, A.; Saremnia, B. Synthesis and characterization of NaA zeolite nanoparticles from Hordeum vulgare L. husk for the separation of total petroleum hydrocarbon by an adsorption process. *J. Taiwan Inst. Chem. Eng.* **2016**, *61*, 276–286. [CrossRef]
138. Terzioğlu, P.; Yücel, S.; Öztürk, M. Application of Box–Behnken design for modeling of lead adsorption onto unmodified and NaCl-modified zeolite NaA obtained from biosilica. *Water Sci. Technol.* **2016**, *75*, 358–365. [CrossRef]
139. Tuaimah, S.K.; Al-Nasri, S.K.; Al-Rahmani, A.A.; abbas, T.K. Using dates leaves midribs to prepare hierarchical structures incorporating porous carbon and zeolite A composites for cesium$^{137}$Cs ion exchange. *Baghdad Sci. J.* **2020**, *17*, 818–825. [CrossRef]
140. Esmaeili, A.; Movahedi Far, F. Synthesis of granular nanozeolite NaA from Phragmites australis for removal of total petroleum hydrocarbon. *Water Qual. Res. J.* **2016**, *51*, 307–320. [CrossRef]
141. Ng, E.-P.; Chow, J.-H.; Mukti, R.R.; Muraza, O.; Ling, T.C.; Wong, K.-L. Hydrothermal synthesis of zeolite a from bamboo leaf biomass and its catalytic activity in cyanoethylation of methanol under autogenic pressure and air conditions. *Mater. Chem. Phys.* **2017**, *201*, 78–85. [CrossRef]
142. Küçük, M.E.; Makarava, I.; Kinnarinen, T.; Häkkinen, A. Simultaneous adsorption of Cu(II), Zn(II), Cd(II) and Pb(II) from synthetic wastewater using NaP and LTA zeolites prepared from biomass fly ash. *Heliyon* **2023**, *9*, e20253. [CrossRef] [PubMed]
143. Azizi, S.N.; Dehnavi, A.R.; Joorabdoozha, A. Synthesis and characterization of LTA nanozeolite using barley husk silica: Mercury removal from standard and real solutions. *Mater. Res. Bull.* **2013**, *48*, 1753–1759. [CrossRef]
144. Moisés, M.P.; da Silva, C.T.P.; Meneguin, J.G.; Girotto, E.M.; Radovanovic, E. Synthesis of zeolite NaA from sugarcane bagasse ash. *Mater. Lett.* **2013**, *108*, 243–246. [CrossRef]
145. Zhao, Y.; Tian, G.; Duan, X.; Liang, X.; Meng, J.; Liang, J. Environmental applications of diatomite minerals in removing heavy metals from water. *Ind. Eng. Chem. Res.* **2019**, *58*, 11638–11652. [CrossRef]
146. Danil de Namor, A.F.; El Gamouz, A.; Frangie, S.; Martinez, V.; Valiente, L.; Webb, O.A. Turning the volume down on heavy metals using tuned diatomite. A review of diatomite and modified diatomite for the extraction of heavy metals from water. *J. Hazard. Mater.* **2012**, *241–242*, 14–31. [CrossRef] [PubMed]
147. Veselý, D.; Kalendova, A.; Kalenda, P. A study of diatomite and calcined kaoline properties in anticorrosion protective coatings. *Prog. Org. Coat.* **2010**, *68*, 173–179. [CrossRef]

148. Nascimento, C.R.; Sobrinho, E.M.O.; Assis, R.B.; Fagundes, R.F.; Bieseki, L.; Pergher, S.B.C. Synthesis of zeolite A using diatomite as silicon and aluminum source. *Cerâmica* **2014**, *60*, 63–68. [CrossRef]
149. El-Kordy, A.; Elgamouz, A.; Abdelhamid, A.; Kawde, A.-N.; Tijani, N.; Lemdek, E.M. Manufacturing of novel zeolite-clay composite membrane from natural clay and diatomite, an electrochemical study of the surface and application towards heavy metals removal. *J. Environ. Chem. Eng.* **2024**, *12*, 112143. [CrossRef]
150. Li, L.; Xu, S.; Liu, Z.; Wang, D. Insight into the growth mechanism of low-temperature synthesis of high-purity lithium slag-based zeolite A. *Materials* **2024**, *17*, 568. [CrossRef]
151. Wu, Z.; Xie, J.; Liu, H.; Chen, T.; Cheng, P.; Wang, C.; Kong, D. Preparation, characterization, and performance of 4A zeolite based on opal waste rock for removal of ammonium ion. *Adsorpt. Sci. Technol.* **2018**, *36*, 1700–1715. [CrossRef]
152. Lei, P.-c.; Shen, X.-j.; Li, Y.; Guo, M.; Zhang, M. An improved implementable process for the synthesis of zeolite 4A from bauxite tailings and its $Cr^{3+}$ removal capacity. *Int. J. Miner. Metall. Mater.* **2016**, *23*, 850–857. [CrossRef]
153. Yan, K.; Zhang, J.; Liu, D.; Meng, X.; Guo, Y.; Cheng, F. Feasible synthesis of magnetic zeolite from red mud and coal gangue: Preparation, transformation and application. *Powder Technol.* **2023**, *423*, 118495. [CrossRef]
154. Kuroki, S.; Hashishin, T.; Morikawa, T.; Yamashita, K.; Matsuda, M. Selective synthesis of zeolites A and X from two industrial wastes: Crushed stone powder and aluminum ash. *J. Environ. Manage.* **2019**, *231*, 749–756. [CrossRef]
155. Terzano, R.; D'Alessandro, C.; Spagnuolo, M.; Romagnoli, M.; Medici, L. Facile zeolite synthesis from municipal glass and aluminum solid wastes. *Clean Soil Air Water* **2015**, *43*, 133–140. [CrossRef]
156. Yao, Z.; Wu, D.; Liu, J.; Wu, W.; Zhao, H.; Tang, J. Recycling of typical difficult-to-treat e-waste: Synthesize zeolites from waste cathode-ray-tube funnel glass. *J. Hazard. Mater.* **2017**, *324*, 673–680. [CrossRef]
157. Lee, W.-H.; Lin, Y.-W.; Lin, K.-L. Parameter optimization, characterization, and crystallization mechanisms underlying the synthesis of zeolite A using liquid crystal display waste glass and sandblasting waste as alternative raw materials. *J. Environ. Chem. Eng.* **2022**, *10*, 108506. [CrossRef]
158. Prasertsab, A.; Leangsiri, W.; Salakhum, S.; Yomthong, K.; Ittisanronnachai, S.; Watcharasing, S.; Kiattikomol, P.; Wattanakit, C. Transformation of production sand waste to FAU and LTA zeolites for selective moisture adsorption and ethanol conversion. *Top. Catal.* **2023**, *66*, 1631–1648. [CrossRef]
159. Tounsi, H.; Mseddi, S.; Djemel, S. Preparation and characterization of Na-LTA zeolite from Tunisian sand and aluminum scrap. *Phys. Procedia* **2009**, *2*, 1065–1074. [CrossRef]
160. Abdelrahman, E.A. Synthesis of zeolite nanostructures from waste aluminum cans for efficient removal of malachite green dye from aqueous media. *J. Mol. Liq.* **2018**, *253*, 72–82. [CrossRef]
161. Ladomerský, J.; Janotka, I.; Hroncová, E.; Najdená, I. One-year properties of concrete with partial substitution of natural aggregate by cupola foundry slag. *J. Cleaner Prod.* **2016**, *131*, 739–746. [CrossRef]
162. Murakami, T.; Sugano, Y.; Kinami, T.; Narushima, T.; Iguchi, Y.; Ouchi, C. Alkali hydrothermal synthesis of zeolite A using oxide by-products. *ISIJ Int.* **2011**, *51*, 158–165. [CrossRef]
163. Sugano, Y.; Sahara, R.; Murakami, T.; Narushima, T.; Iguchi, Y.; Ouchi, C. Hydrothermal synthesis of zeolite A using blast furnace slag. *ISIJ Int.* **2005**, *45*, 937–945. [CrossRef]
164. Anuwattana, R.; Khummongkol, P. Conventional hydrothermal synthesis of Na-A zeolite from cupola slag and aluminum sludge. *J. Hazard. Mater.* **2009**, *166*, 227–232. [CrossRef] [PubMed]
165. Li, C.; Li, X.; Li, C.; Li, L. Synthesis, characterization of NaA zeolite from blast furnace slag (BFS) via alkaline fusion and hydrothermal treatment. *J. Wuhan Univ. Technol. Mater. Sci. Ed.* **2023**, *38*, 401–407. [CrossRef]
166. Singh, S.K.; Rekha, P.; Surya, M. Utilization of Linz–Donawitz slag from steel industry for waste minimization. *J. Mater. Cycles Waste Manage.* **2020**, *22*, 611–627. [CrossRef]
167. Samanta, N.S.; Banerjee, S.; Mondal, P.; Anweshan; Bora, U.; Purkait, M.K. Preparation and characterization of zeolite from waste Linz-Donawitz (LD) process slag of steel industry for removal of $Fe^{3+}$ from drinking water. *Adv. Powder Technol.* **2021**, *32*, 3372–3387. [CrossRef]
168. Samanta, N.S.; Das, P.P.; Mondal, P.; Bora, U.; Purkait, M.K. Physico-chemical and adsorption study of hydrothermally treated zeolite A and FAU-type zeolite X prepared from LD (Linz–Donawitz) slag of the steel industry. *Int. J. Environ. Anal. Chem.* **2024**, *104*, 3219–3241. [CrossRef]
169. Cheng, X.-w.; Zhong, Y.; Wang, J.; Guo, J.; Huang, Q.; Long, Y.-c. Studies on modification and structural ultra-stabilization of natural STI zeolite. *Microporous Mesoporous Mater.* **2005**, *83*, 233–243. [CrossRef]
170. Wang, S.; Peng, Y. Natural zeolites as effective adsorbents in water and wastewater treatment. *Chem. Eng. J.* **2010**, *156*, 11–24. [CrossRef]
171. Faghihian, H.; Maragheh, M.G.; Amini, M.K.; Nezamzadeh, A.R. Thorium ion uptake by zeolite a synthesized from natural clinoptilolite tuffs. *Adsorpt. Sci. Technol.* **2004**, *22*, 707–717. [CrossRef]
172. Faghihian, H.; Amini, M.K.; Nezamzadeh, A.R. Cerium uptake by zeolite A synthesized from natural clinoptilolite tuffs. *J. Radioanal. Nucl. Chem.* **2005**, *264*, 577–582. [CrossRef]

173. Kazemian, H.; Modarress, H.; Kazemi, M.; Farhadi, F. Synthesis of submicron zeolite LTA particles from natural clinoptilolite and industrial grade chemicals using one stage procedure. *Powder Technol.* **2009**, *196*, 22–25. [CrossRef]
174. Yue, M.B.; Huang, L.; Dong, X.; Xu, J.H.; Zhu, J.H. Attempts to synthesize zeolitic composites from stellerite. *Mater. Manuf. Processes* **2007**, *22*, 700–704. [CrossRef]
175. Pathak, A.; Rana, M.S.; Marafi, M.; Kothari, R.; Gupta, P.; Tyagi, V.V. Waste petroleum fluid catalytic cracking catalysts as a raw material for synthesizing valuable zeolites: A critical overview on potential, applications, and challenges. *Sustainable Mater. Technol.* **2023**, *38*, e00733. [CrossRef]
176. Zhang, L.; Hu, Q.; Qin, Y.; Liu, H.; Zhao, X.; Gao, X.; Song, L.; Sun, Z. Optimized zeolite distribution of FCC catalysts for promoting heavy-oil catalytic cracking. *Ind. Eng. Chem. Res.* **2022**, *61*, 11628–11635. [CrossRef]
177. Gonzalez, M.R.; Pereyra, A.M.; Zerbino, R.; Basaldella, E.I. Removal and cementitious immobilization of heavy metals: Chromium capture by zeolite-hybridized materials obtained from spent fluid cracking catalysts. *J. Cleaner Prod.* **2015**, *91*, 187–190. [CrossRef]
178. Gonzalez, M.R.; Pereyra, A.M.; Bosch, P.; Fetter, G.; Lara, V.H.; Basaldella, E.I. Structural and morphological evolutions of spent FCC catalyst pellets toward NaA zeolite. *J. Mater. Sci.* **2016**, *51*, 5061–5072. [CrossRef]
179. Monzón, J.D.; Gonzalez, M.R.; Mardones, L.E.; Conconi, M.S.; Pereyra, A.M.; Basaldella, E.I. The role of alkaline activation in the structural transformations of aluminosiliceous industrial wastes towards zeolite production. *Mater. Today Commun.* **2019**, *21*, 100624. [CrossRef]
180. Mallapur, V.P.; Oubagaranadin, J.U.K. A brief review on the synthesis of zeolites from hazardous wastes. *Trans. Indian Ceram. Soc.* **2017**, *76*, 1–13. [CrossRef]
181. Wajima, T.; Ikegami, Y. Synthesis of zeolitic materials from waste porcelain at low temperature via a two-step alkali conversion. *Ceram. Int.* **2007**, *33*, 1269–1274. [CrossRef]
182. Nezamzadeh-Ejhieh, A.; Banan, Z. A comparison between the efficiency of CdS nanoparticles/zeolite A and CdO/zeolite A as catalysts in photodecolorization of crystal violet. *Desalination* **2011**, *279*, 146–151. [CrossRef]
183. Li, W.; Jin, H.; Xie, H.; Wang, D. Progress in comprehensive utilization of electrolytic manganese residue: A review. *Environ. Sci. Pollut. Res.* **2023**, *30*, 48837–48853. [CrossRef] [PubMed]
184. Li, W.; Jin, H.; Xie, H.; Ma, L. Synthesis of zeolite A and zeolite X from electrolytic manganese residue, its characterization and performance for the removal of $Cd^{2+}$ from wastewater. *Chin. J. Chem. Eng.* **2023**, *62*, 31–45. [CrossRef]
185. Li, W.; Jin, H.; Xie, H.; Wang, D.; Lei, E. Utilization of electrolytic manganese residue to synthesize zeolite A and zeolite X for Mn ions adsorption. *J. Ind. Eng. Chem.* **2023**, *120*, 147–158. [CrossRef]
186. Li, W.; Jin, H.; Xie, H.; Wang, M.; Han, Y. Utilization of electrolytic manganese residue and bauxite to synthesize zeolite a for pickle liquor adsorption: Characterization, mechanisms and performance. *J. Cleaner Prod.* **2023**, *429*, 139537. [CrossRef]
187. Kasai, M.; Kobayashi, Y.; Yoshida, K.; Sasaki, Y.; Togo, M.; Nakahira, A. Synthesis and evaluation of zeolite surface-modified perlite. *J. Ceram. Soc. Jpn.* **2018**, *126*, 115–121. [CrossRef]
188. Monzón, J.D.; Gonzalez, M.R.; Muñoz, M.; Pereyra, A.M.; Basaldella, E.I. Phase-transition process in the hydrothermal zeolitization of volcanic ash into LTA and FAU structures. *Clays Clay Miner.* **2021**, *69*, 735–745. [CrossRef]
189. Meng, Q.; Chen, H.; Lin, J.; Lin, Z.; Sun, J. Zeolite A synthesized from alkaline assisted pre-activated halloysite for efficient heavy metal removal in polluted river water and industrial wastewater. *J. Environ. Sci.* **2017**, *56*, 254–262. [CrossRef] [PubMed]
190. Zhao, Y.; Zhang, B.; Zhang, X.; Wang, J.; Liu, J.; Chen, R. Preparation of highly ordered cubic NaA zeolite from halloysite mineral for adsorption of ammonium ions. *J. Hazard. Mater.* **2010**, *178*, 658–664. [CrossRef]
191. Fernandes-Machado, N.R.C.; Miotto-Bigatão, D.M.M. Utilização de zeólitas sintetizadas a partir de xisto retortado na remoção de arsênio em águas contaminadas. *Quim. Nova* **2007**, *30*, 1108–1114. [CrossRef]
192. Miyake, M.; Tamura, C.; Matsuda, M. Resource recovery of waste incineration fly ash: Synthesis of zeolites A and P. *J. Am. Ceram. Soc.* **2002**, *85*, 1873–1875. [CrossRef]
193. Tamura, C.; Matsuda, M.; Miyake, M. Conversion of waste incineration fly ash into zeolite A and zeolite P by hydrothermal treatment. *J. Ceram. Soc. Jpn.* **2007**, *114*, 205–209. [CrossRef]
194. Xie, W.-M.; Zhou, F.-P.; Bi, X.-L.; Chen, D.-D.; Li, J.; Sun, S.-Y.; Liu, J.-Y.; Chen, X.-Q. Accelerated crystallization of magnetic 4A-zeolite synthesized from red mud for application in removal of mixed heavy metal ions. *J. Hazard. Mater.* **2018**, *358*, 441–449. [CrossRef]
195. Joseph, I.V.; Roncaglia, G.; Tosheva, L.; Doyle, A.M. Waste peat ash mineralogy and transformation to microporous zeolites. *Fuel Process. Technol.* **2019**, *194*, 106124. [CrossRef]
196. Cui, K.-B.; Lyu, J.-W.; Liu, H.-Z.; Yang, J.-L.; Yan, Z.-Q.; Yang, W.; Liu, X.; Qiu, J. Eco-friendly synthesis of magnetic zeolite A from red mud and coal gasification slag for the removal of $Pb^{2+}$ and $Cu^{2+}$. *J. Environ. Chem. Eng.* **2024**, *12*, 113739. [CrossRef]
197. Belaabed, R.; El Knidri, H.; Addaou, A.; Laajeb, A.; Lahsini, A. Optimization of zeolite LTA synthesis parameters for chromium removal from tannery wastewater. *Chem. Afr.* **2024**, *7*, 3329–3341. [CrossRef]
198. Wang, M.; Xu, D.; Ma, H.; Li, B.; Howard, A. Synthesis of NaA zeolite from foundry dust and its adsorption capacity of ammonia. *J. Environ. Manag.* **2023**, *331*, 117297. [CrossRef]

199. Corma, A.; Rey, F.; Rius, J.; Sabater, M.J.; Valencia, S. Supramolecular self-assembled molecules as organic directing agent for synthesis of zeolites. *Nature* **2004**, *431*, 287–290. [CrossRef]
200. Boal, B.W.; Schmidt, J.E.; Deimund, M.A.; Deem, M.W.; Henling, L.M.; Brand, S.K.; Zones, S.I.; Davis, M.E. Facile synthesis and catalysis of pure-silica and heteroatom LTA. *Chem. Mater.* **2015**, *27*, 7774–7779. [CrossRef]
201. Cheung, O.; Bacsik, Z.; Fil, N.; Krokidas, P.; Wardecki, D.; Hedin, N. Selective adsorption of $CO_2$ on zeolites NaK-ZK-4 with Si/Al of 1.8-2.8. *ACS Omega* **2020**, *5*, 25371–25380. [CrossRef] [PubMed]
202. Rigo, R.T.; Prigol, C.; Antunes, A. Synthesis of ZK4 zeolite: An LTA-structured zeolite with a Si/Al ratio greater than 1. *Mater. Lett.* **2013**, *102*, 87–90. [CrossRef]
203. Tao, Z.; Tian, Y.; Ou, S.Y.; Gu, Q.; Shang, J. Direct air capture of $CO_2$ by metal cation-exchanged LTA zeolites: Effect of the charge-to-size ratio of cations. *AIChE J.* **2023**, *69*, 10. [CrossRef]
204. Ahn, N.H.; Ryu, T.; Kang, Y.; Kim, H.; Shin, J.; Nam, I.-S.; Hong, S.B. The origin of an unexpected increase in $NH_3$–SCR activity of aged Cu-LTA catalysts. *ACS Catal.* **2017**, *7*, 6781–6785. [CrossRef]
205. Jo, D.; Park, G.T.; Ryu, T.; Hong, S.B. Economical synthesis of high-silica LTA zeolites: A step forward in developing a new commercial $NH_3$-SCR catalyst. *Appl. Catal., B* **2019**, *243*, 212–219. [CrossRef]
206. Park, M.B.; Lee, Y.; Zheng, A.; Xiao, F.-S.; Nicholas, C.P.; Lewis, G.J.; Hong, S.B. Formation pathway for LTA zeolite crystals synthesized via a charge density mismatch approach. *J. Am. Chem. Soc.* **2013**, *135*, 2248–2255. [CrossRef] [PubMed]
207. Ryu, T.; Ahn, N.H.; Seo, S.; Cho, J.; Kim, H.; Jo, D.; Park, G.T.; Kim, P.S.; Kim, C.H.; Bruce, E.L.; et al. Fully copper-exchanged high-silica LTA zeolites as unrivaled hydrothermally stable $NH_3$-SCR catalysts. *Angew. Chem. Int. Ed.* **2017**, *56*, 3256–3260. [CrossRef] [PubMed]
208. Ryu, T.; Kim, H.; Hong, S.B. Nature of active sites in Cu-LTA $NH_3$-SCR catalysts: A comparative study with Cu-SSZ-13. *Appl. Catal., B* **2019**, *245*, 513–521. [CrossRef]
209. Wang, Y.; Li, X.; Liu, X.; Song, X.; Zeng, S.; Wang, B.; Li, X.; Tao, S. Construction of the mosaic aluminophosphate zeotypes based on nonclassical crystallization and in situ selective etching strategies. *Microporous Mesoporous Mater.* **2024**, *367*, 112999. [CrossRef]
210. Lin, Y.; Guo, K.; Wang, M.; Tao, S.; Zhang, L.; Wei, Y. Tetraalkylammonium hydroxide-assisted ionothermal synthesis and characterization of LTA-type aluminophosphate zeotypes with high structural stability after detemplation and hydration. *New J. Chem.* **2018**, *42*, 15453–15459. [CrossRef]
211. Li, L.; Li, X.; Wang, B.; Zi, W.; Ji, Q.; Li, Y.; Zhang, X.; Wang, Y.; Ding, Y.; Liu, J.; et al. Ultrafast synthesis of discrete submicron $AlPO_4$-LTA molecular sieve crystals and their application in molecular sieve membrane. *Microporous Mesoporous Mater.* **2022**, *334*, 111771. [CrossRef]
212. Krajnc, A.; Varlec, J.; Mazaj, M.; Ristić, A.; Logar, N.Z.; Mali, G. Superior performance of microporous aluminophosphate with LTA topology in solar-energy storage and heat reallocation. *Adv. Energy Mater.* **2017**, *7*, 1601815. [CrossRef]
213. Huang, A.; Caro, J. Preparation of large and well-shaped LTA-type $AlPO_4$ crystals by using crown ether Kryptofix 222 as structure directing agent. *Microporous Mesoporous Mater.* **2010**, *129*, 90–99. [CrossRef]
214. Azim, M.M.; Mohsin, U. An efficient method for the ionothermal synthesis of aluminophospahte with the LTA framework type. *Microporous Mesoporous Mater.* **2020**, *295*, 109957. [CrossRef]
215. Xu, X.T.; Zhai, J.P.; Chen, Y.P.; Li, I.L.; Chen, H.Y.; Ruan, S.C.; Tang, Z.K. Synthesis of large single crystals of AlPO–LTA by using n-Propylamine as structure directing agent. *J. Cryst. Growth* **2014**, *407*, 1–5. [CrossRef]
216. Pinilla-Herrero, I.; Márquez-Álvarez, C.; Sastre, E. Complex relationship between SAPO framework topology, content and distribution of Si and catalytic behaviour in the MTO reaction. *Catal. Sci. Technol.* **2017**, *7*, 3892–3901. [CrossRef]
217. Pinilla-Herrero, I.; Olsbye, U.; Márquez-Álvarez, C.; Sastre, E. Effect of framework topology of SAPO catalysts on selectivity and deactivation profile in the methanol-to-olefins reaction. *J. Catal.* **2017**, *352*, 191–207. [CrossRef]
218. Lin, Y.; Wei, Y.; Zhang, L.; Guo, K.; Wang, M.; Huang, P.; Meng, X.; Zhang, R. Facile ionothermal synthesis of SAPO-LTA zeotypes with high structural stability and their catalytic performance in MTO reaction. *Microporous Mesoporous Mater.* **2019**, *288*, 109611. [CrossRef]
219. Vinaches, P.; Pergher, S.B.C. Organic structure-directing agents in SAPO synthesis: The case of 2-Ethyl-1,3,4-trimethylimidazolium. *Eur. J. Inorg. Chem.* **2018**, *2018*, 122. [CrossRef]
220. Martínez-Franco, R.; Cantín, Á.; Vidal-Moya, A.; Moliner, M.; Corma, A. Self-assembled aromatic molecules as efficient organic structure directing agents to synthesize the silicoaluminophosphate SAPO-42 with isolated Si species. *Chem. Mater.* **2015**, *27*, 2981–2989. [CrossRef]
221. Zhang, H.; Huo, S.; Yeager, K.; Xi, B.; Zhang, J.; He, Z.; Ma, C.; Wu, F. Accumulation of arsenic, mercury and heavy metals in lacustrine sediment in relation to eutrophication: Impacts of sources and climate change. *Ecol. Indic.* **2018**, *93*, 771–780. [CrossRef]
222. Liu, Y.; Zhou, Z.; Gong, W.; Xu, Y.; Ding, Q.; Cui, L. Distribution, risk assessment of heavy metals in sediments, and their potential risk on water supply safety of a drinking water reservoir, middle China. *Environ. Sci. Pollut. Res. Int.* **2023**, *30*, 73702–73713. [CrossRef] [PubMed]

223. He, J.; Shi, D.; Wang, B.-B.; Feng, C.-L.; Su, H.-L.; Wang, Y.; Qin, N. Ecological risk assessment and water quality standard evaluation of 10 typical metals in eight basins in China. *China Environ. Sci.* **2019**, *39*, 2970–2982.
224. Cui, W.; Tang, K.; Chen, Y.; Chen, Z.; Lan, Y.; Hong, Y.; Lan, W. Regulating the particle sizes of NaA molecular sieves toward enhanced heavy metal ion adsorption. *New J. Chem.* **2024**, *48*, 7863–7874. [CrossRef]
225. Nseke, J.M.; Baloyi, N.P. Ecofriendly synthesized Zeolite 4A for the treatment of a multi-cationic contaminant-based effluent: Central composite design (CCD) statistical approach. *Heliyon* **2024**, *10*, e35176. [CrossRef] [PubMed]
226. Mubarak, M.F.; Mohamed, A.M.G.; Keshawy, M.; elMoghny, T.A.; Shehata, N. Adsorption of heavy metals and hardness ions from groundwater onto modified zeolite: Batch and column studies. *Alexandria Eng. J.* **2022**, *61*, 4189–4207. [CrossRef]
227. Ghasemi, M.; Javadian, H.; Ghasemi, N.; Agarwal, S.; Gupta, V.K. Microporous nanocrystalline NaA zeolite prepared by microwave assisted hydrothermal method and determination of kinetic, isotherm and thermodynamic parameters of the batch sorption of Ni (II). *J. Mol. Liq.* **2016**, *215*, 161–169. [CrossRef]
228. Rentsennorov, U.; Davaabal, B.; Dovchin, B.; Temuujin, J. Adsorption of Cr(III) from aqueous media on zeolite a prepared from fused fly ash by hydrothermal synthesis. *J. Ceram. Process. Res.* **2021**, *22*, 232–239.
229. Xiao, M.; Hu, X.; Gong, Y.; Gao, D.; Zhang, P.; Liu, Q.; Liu, Y.; Wang, M. Solid transformation synthesis of zeolites from fly ash. *RSC Adv.* **2015**, *5*, 100743–100749. [CrossRef]
230. Guan, Q.; Gao, K.; Ning, P.; Miao, R.; He, L. Efficient removal of low-concentration Cr(VI) from aqueous solution by 4A/HACC particles. *New J. Chem.* **2019**, *43*, 17220–17230. [CrossRef]
231. Li, Y.; Yang, L.; Li, X.; Miki, T.; Nagasaka, T. A composite adsorbent of ZnS nanoclusters grown in zeolite NaA synthesized from fly ash with a high mercury ion removal efficiency in solution. *J. Hazard. Mater.* **2021**, *411*, 125044. [CrossRef] [PubMed]
232. Fang, X.; Xu, Z.; Luo, Y.; Ren, L.; Hua, W. Removal of radionuclides from laundry wastewater containing organics and suspended solids using inorganic ion exchanger. *Procedia Environ. Sci.* **2016**, *31*, 375–381. [CrossRef]
233. Murukutti, M.K.; Jena, H. Synthesis of nano-crystalline zeolite-A and zeolite-X from Indian coal fly ash, its characterization and performance evaluation for the removal of $Cs^{+}$ and $Sr^{2+}$ from simulated nuclear waste. *J. Hazard. Mater.* **2022**, *423*, 127085. [CrossRef] [PubMed]
234. Lee, H.Y.; Kim, H.S.; Jeong, H.-K.; Park, M.; Chung, D.-Y.; Lee, K.-Y.; Lee, E.-H.; Lim, W.T. Selective removal of radioactive cesium from nuclear waste by zeolites: On the origin of cesium selectivity revealed by systematic crystallographic studies. *J. Phys. Chem. C* **2017**, *121*, 10594–10608. [CrossRef]
235. Hao, W.; Yan, N.; Xie, M.; Yan, X.; Guo, X.; Bai, P.; Guo, P.; Cheng, T.; Yan, W. Origin of the exceptional selectivity of NaA zeolite for the radioactive isotope $^{90}Sr^{2+}$. *Inorg. Chem. Front.* **2022**, *9*, 6258–6270. [CrossRef]
236. Dahake, R.; Tiwari, P.; Bansiwal, A. Multicycle adsorption and desorption for recovery of U(VI) from aqueous solution using oxime modified zeolite-A. *J. Radioanal. Nucl. Chem.* **2021**, *327*, 133–142. [CrossRef]
237. Park, J.-S.; Song, J.-H.; Yeon, K.-H.; Moon, S.-H. Removal of hardness ions from tap water using electromembrane processes. *Desalination* **2007**, *202*, 1–8. [CrossRef]
238. Alshameri, A.; Ibrahim, A.; Assabri, A.M.; Lei, X.; Wang, H.; Yan, C. The investigation into the ammonium removal performance of Yemeni natural zeolite: Modification, ion exchange mechanism, and thermodynamics. *Powder Technol.* **2014**, *258*, 20–31. [CrossRef]
239. Kusrini, E.; Mualim, N.M.; Rahman, A.; Usman, A.; Nugraha, I.G.D. Application of activated Na-zeolite a as a water softening agent to remove $Ca^{2+}$ and $Mg^{2+}$ ions from water. *AIP Conf. Proc.* **2020**, *2255*, 1–5.
240. Manna, M.; Sen, S. Tuning crystallization for controlled morphology of zeolite A by an eco-friendly sonochemical precursor-less method. *Mater. Chem. Phys.* **2023**, *309*, 128378. [CrossRef]
241. El-Nahas, S.; Osman, A.I.; Arafat, A.S.; Al-Muhtaseb, A.a.H.; Salman, H.M. Facile and affordable synthetic route of nano powder zeolite and its application in fast softening of water hardness. *J. Water Process Eng.* **2020**, *33*, 101104. [CrossRef]
242. Xue, Z.; Li, Z.; Ma, J.; Bai, X.; Kang, Y.; Hao, W.; Li, R. Effective removal of $Mg^{2+}$ and $Ca^{2+}$ ions by mesoporous LTA zeolite. *Desalination* **2014**, *341*, 10–18. [CrossRef]
243. Painer, F.; Baldermann, A.; Gallien, F.; Eichinger, S.; Steindl, F.; Dohrmann, R.; Dietzel, M. Synthesis of zeolites from fine-grained perlite and their application as sorbents. *Materials* **2022**, *15*, 4474. [CrossRef] [PubMed]
244. Wang, P.; Sun, Q.; Zhang, Y.; Cao, J. Alkali-dissolving hydrothermal synthesis of zeolite P from fly ash. *Micro Nano Lett.* **2019**, *14*, 572–576. [CrossRef]
245. Randall, D.J.; Tsui, T.K.N. Ammonia toxicity in fish. *Mar. Pollut. Bull.* **2002**, *45*, 17–23. [CrossRef]
246. Qin, W.; Wei, S.P.; Zheng, Y.; Choi, E.; Li, X.; Johnston, J.; Wan, X.; Abrahamson, B.; Flinkstrom, Z.; Wang, B.; et al. Ammonia-oxidizing bacteria and archaea exhibit differential nitrogen source preferences. *Nat. Microbiol.* **2024**, *9*, 524–536. [CrossRef] [PubMed]
247. Ren, X.; Xiao, L.; Qu, R.; Liu, S.; Ye, D.; Song, H.; Wu, W.; Zheng, C.; Wu, X.; Gao, X. Synthesis and characterization of a single phase zeolite A using coal fly ash. *RSC Adv.* **2018**, *8*, 42200–42209. [CrossRef]

248. Jiang, Q.; He, J.; Wang, Y.; Chen, B.; Tian, K.; Yang, K.; Wei, H.; Xu, X. Efficient removal of ammonia–nitrogen in wastewater by zeolite molecular sieves prepared from coal fly ash. *Sci. Rep.* **2024**, *14*, 21064. [CrossRef] [PubMed]
249. Wang, X.; Zhang, Y. Synthesis and characterization of zeolite A obtained from coal gangue for the adsorption of $F^-$ in wastewater. *Sci. Adv. Mater.* **2019**, *11*, 277–282. [CrossRef]
250. Naskar, M.K. Preparation of colloidal hydrated alumina modified NaA zeolite derived from rice husk ash for effective removal of fluoride ions from water medium. *J. Asian Ceram. Soc.* **2020**, *8*, 437–447. [CrossRef]
251. Chakraborty, A.; Naskar, M.K. Study on the synthesis and structural properties of zeolite A-MgO composite for defluoridation of water. *Trans. Indian Ceram. Soc.* **2021**, *80*, 199–207. [CrossRef]
252. Kugbe, J.; Matsue, N.; Henmi, T. Synthesis of Linde type A zeolite–goethite nanocomposite as an adsorbent for cationic and anionic pollutants. *J. Hazard. Mater.* **2009**, *164*, 929–935. [CrossRef]
253. Guan, Q.; Deng, L.; Zhang, D.; Ning, P.; Kong, Z.; He, L. Preparation of tetraethylenepentamine-functionalized 4A zeolite for effective removal of phosphate in water. *Appl. Organomet. Chem.* **2020**, *34*, e5861. [CrossRef]
254. Pillewan, P.; Mukherjee, S.; Meher, A.K.; Rayalu, S.; Bansiwal, A. Removal of arsenic (III) and arsenic (V) using copper exchange zeolite-A. *Environ. Prog. Sustain. Energy* **2014**, *33*, 1274–1282. [CrossRef]
255. Abukhadra, M.R.; Mostafa, M.; Jumah, M.N.B.; Al-Khalawi, N.; Alruhaimi, R.S.; Salama, Y.F.; Allam, A.A. Insight into the adsorption properties of chitosan/Zeolite-A hybrid structure for effective decontamination of toxic Cd (II) and As (V) ions from the aqueous environments. *J. Polym. Environ.* **2022**, *30*, 295–307. [CrossRef]
256. Ashraf, M.-T.; AlHammadi, A.A.; El-Sherbeeny, A.M.; Alhammadi, S.; Al Zoubi, W.; Ko, Y.G.; Abukhadra, M.R. Synthesis of cellulose fibers/Zeolite-A nanocomposite as an environmental adsorbent for organic and inorganic selenium ions; Characterization and advanced equilibrium studies. *J. Mol. Liq.* **2022**, *360*, 119573. [CrossRef]
257. Haghjoo, S.; Lengauer, C.L.; Kazemian, H.; Roushani, M. Facile and innovative application of surfactant-modified-zeolite from Austrian fly ash for glyphosate removal from water solution. *J. Environ. Manage.* **2023**, *346*, 118976. [CrossRef] [PubMed]
258. Kamgang Djioko, F.H.; Fotsop, C.G.; Kamgang Youbi, G.; Nwanonenyi, S.C.; Oguzie, E.E.; Ada Madu, C. Efficient removal of pharmaceutical contaminant in wastewater using low-cost zeolite 4A derived from kaolin: Experimental and theoretical studies. *Mater. Chem. Phys.* **2024**, *315*, 128994. [CrossRef]
259. Mostafa, M.; Bin Jumah, M.N.; Othman, S.I.; Alruhaimi, R.S.; Salama, Y.F.; Allam, A.A.; Abukhadra, M.R. Effective removal of different species of organophosphorus pesticides (acephate, omthosate, and methyl parathion) using chitosan/zeolite-A as multifunctional adsorbent. *Environ. Technol. Innov.* **2021**, *24*, 101875. [CrossRef]
260. Muniandy, S.; Salleh, L.; Zaini, M.A.A. Evaluation of malachite green and methyl violet dyes removal by 3A molecular sieve adsorbents. *Desalin. Water Treat.* **2020**, *203*, 440–448. [CrossRef]
261. Xu, H.; Wu, L.; Shi, T.; Liu, W.; Qi, S. Adsorption of acid fuchsin onto LTA-type zeolite derived from fly ash. *Sci. China Technol. Sci.* **2014**, *57*, 1127–1134. [CrossRef]
262. Nyankson, E.; Adjasoo, J.; Efavi, J.K.; Amedalor, R.; Yaya, A.; Manu, G.P.; Asare, K.; Amartey, N.A. Characterization and evaluation of zeolite A/$Fe_3O_4$ nanocomposite as a potential adsorbent for removal of organic molecules from wastewater. *J. Chem.* **2019**, *2019*, 8090756. [CrossRef]
263. Elfeky, A.S.; Youssef, H.F.; Elzaref, A.S. Adsorption of dye from wastewater onto ZnO nanoparticles-loaded zeolite: Kinetic, thermodynamic and isotherm studies. *Z. Phys. Chem.* **2020**, *234*, 255–278. [CrossRef]
264. Khalaf, I.H.; Al-Sudani, F.T.; AbdulRazak, A.A.; Aldahri, T.; Rohani, S. Optimization of Congo red dye adsorption from wastewater by a modified commercial zeolite catalyst using response surface modeling approach. *Water Sci. Technol.* **2021**, *83*, 1369–1383. [CrossRef] [PubMed]
265. Kwon, S.; Choi, Y.; Singh, B.K.; Na, K. Selective and rapid capture of $Sr^{2+}$ with LTA zeolites: Effect of crystal sizes and mesoporosity. *Appl. Surf. Sci.* **2020**, *506*, 145029. [CrossRef]
266. Merceille, A.; Weinzaepfel, E.; Barré, Y.; Grandjean, A. The sorption behaviour of synthetic sodium nonatitanate and zeolite A for removing radioactive strontium from aqueous wastes. *Sep. Purif. Technol.* **2012**, *96*, 81–88. [CrossRef]
267. Chen, Z.; Li, X.; Liu, H.; Xu, W.; Yu, J.; Zang, Y.; Hu, G.; Hu, T.; Jiang, J.; Mao, P.; et al. A novel and cost-effective synthesis of magnetic zeolite 4A using kaolinite and red mud for Sr(II) removal. *Microporous Mesoporous Mater.* **2024**, *370*, 113069. [CrossRef]
268. Faghihian, H.; Moayed, M.; Firooz, A.; Iravani, M. Synthesis of a novel magnetic zeolite nanocomposite for removal of $Cs^+$ and $Sr^{2+}$ from aqueous solution: Kinetic, equilibrium, and thermodynamic studies. *J. Colloid Interface Sci.* **2013**, *393*, 445–451. [CrossRef] [PubMed]
269. Huang, Y.-H.; Wu, Y.-C. Highly efficient adsorption of $Sr^{2+}$ and $Co^{2+}$ ions by ambient prepared alkali activated metakaolin. *Polymers* **2022**, *14*, 992. [CrossRef] [PubMed]
270. Liu, H.; Peng, S.; Shu, L.; Chen, T.; Bao, T.; Frost, R.L. Magnetic zeolite NaA: Synthesis, characterization based on metakaolin and its application for the removal of $Cu^{2+}$, $Pb^{2+}$. *Chemosphere* **2013**, *91*, 1539–1546. [CrossRef]
271. Jangkorn, S.; Youngme, S.; Praipipat, P. Comparative lead adsorptions in synthetic wastewater by synthesized zeolite A of recycled industrial wastes from sugar factory and power plant. *Heliyon* **2022**, *8*, e09323. [CrossRef] [PubMed]

272. Rayalu, S.; Dhopte, S.D.; Kumar, P. Flyash based zeolite-A:A suitable sorbent for lead removal. *Indian J. Chem. Technol.* **2004**, *11*, 227–233.
273. Su, Q.; He, Y.; Yang, S.; Wan, H.; Chang, S.; Cui, X. Synthesis of NaA-zeolite microspheres by conversion of geopolymer and their performance of Pb (II) removal. *Appl. Clay Sci.* **2021**, *200*, 105914. [CrossRef]
274. Wei, E.; Wang, K.; Muhammad, Y.; Chen, S.; Dong, D.; Wei, Y.; Fujita, T. Preparation and conversion mechanism of different geopolymer-based zeolite microspheres and their adsorption properties for $Pb^{2+}$. *Sep. Purif. Technol.* **2022**, *282*, 119971. [CrossRef]
275. Lv, Y.; Ma, B.; Liu, Y.; Wang, C.; Chen, Y. Adsorption behavior and mechanism of mixed heavy metal ions by zeolite adsorbent prepared from lithium leach residue. *Microporous Mesoporous Mater.* **2022**, *329*, 111553. [CrossRef]
276. Cheng, J.; Hua, X.; Zhang, G.; Yu, M.; Wang, Z.; Zhang, Y.; Liu, W.; Chen, Y.; Wang, H.; Luo, Y.; et al. Synthesis of high-crystallinity zeolite A from rare earth tailings: Investigating adsorption performance on typical pollutants in rare earth mines. *J. Hazard. Mater.* **2024**, *468*, 133730. [CrossRef] [PubMed]
277. Hashemi, S.M.; Salehirad, A.; Nasri, Z. Preparation of zeolite A by inorganic complex precursor route for efficient elimination of heavy metal cations from aqueous solutions. *Inorg. Nano-Met. Chem.* **2023**, *53*, 66–77. [CrossRef]
278. Ahmed, I.M.; Attia, L.A.; Attallah, M.F. Modification of perlite to prepare low cost zeolite as adsorbent material for removal of $^{144}Ce$ and $^{152+154}Eu$ from aqueous solution. *Radiochim. Acta* **2020**, *108*, 727–735. [CrossRef]
279. Torad, N.L.; Naito, M.; Tatami, J.; Endo, A.; Leo, S.-Y.; Ishihara, S.; Wu, K.C.W.; Wakihara, T.; Yamauchi, Y. Highly crystallized nanometer-sized zeolite A with large Cs adsorption capability for the decontamination of water. *Chem. Asian J.* **2014**, *9*, 759–763. [CrossRef] [PubMed]
280. Ma, S.; Yang, H.; Fu, S.; Hu, Y.; He, P.; Sun, Z.; Duan, X.; Jia, D.; Colombo, P.; Zhou, Y. Additive manufacturing of hierarchical Zeolite-A lattices with exceptionally high $Cs^+$ adsorption capacity and near-unity immobilization efficiency. *Chem. Eng. J.* **2023**, *474*, 145909. [CrossRef]
281. Faghihian, H.; Iravani, M.; Moayed, M.; Ghannadi-Maragheh, M. Preparation of a novel PAN-zeolite nanocomposite for removal of $Cs^+$ and $Sr^{2+}$ from aqueous solutions: Kinetic, equilibrium, and thermodynamic studies. *Chem. Eng. J.* **2013**, *222*, 41–48. [CrossRef]
282. Vipin, A.K.; Ling, S.; Fugetsu, B. Removal of $Cs^+$ and $Sr^{2+}$ from water using MWCNT reinforced zeolite-A beads. *Microporous Mesoporous Mater.* **2016**, *224*, 84–88. [CrossRef]
283. Tian, Q.; Sasaki, K. Application of fly ash-based materials for stabilization/solidification of cesium and strontium. *Environ. Sci. Pollut. Res.* **2019**, *26*, 23542–23554. [CrossRef] [PubMed]
284. Salimkhani, S.; Siahcheshm, K.; Kadkhodaie, A.; Salimkhani, H. Structural analysis and the effect of the chromium on LTA (Na) zeolite synthesized from kaolin. *Mater. Chem. Phys.* **2021**, *271*, 124957. [CrossRef]
285. Derbe, T.; Zereffa, E.A.; Sani, T. Synthesis of zeolite-A/$Fe_3O_4$/biochar composite for removal of Cr(VI) from aqueous solution. *Int. J. Environ. Sci. Technol.* **2024**, *21*, 10027–10046. [CrossRef]
286. Ayele, L.; Pérez, E.; Mayoral, Á.; Chebude, Y.; Díaz, I. Synthesis of zeolite A using raw kaolin from Ethiopia and its application in removal of Cr(III) from tannery wastewater. *J. Chem. Technol. Biotechnol.* **2018**, *93*, 146–154. [CrossRef]
287. Yoon, S.-Y.; Lee, C.-G.; Kim, J.-H.; Kang, J.-K.; Park, J.-A.; Kim, S.-B. Characterization of magnetic zeolite-polymer composites for Cu(II) and Cr(III) removal from aqueous solutions. *Desalin. Water Treat.* **2017**, *67*, 261–270. [CrossRef]
288. Miyake, M.; Jha, V.K.; Kimura, Y.; Matsuda, M. Effective utilization of coal fly ash containing unburned carbon. *WIT Trans. Ecol. Environ.* **2009**, *109*, 203–212.
289. Abdelrahman, E.A.; Abou El-Reash, Y.G.; Youssef, H.M.; Kotp, Y.H.; Hegazey, R.M. Utilization of rice husk and waste aluminum cans for the synthesis of some nanosized zeolite, zeolite/zeolite, and geopolymer/zeolite products for the efficient removal of Co(II), Cu(II), and Zn(II) ions from aqueous media. *J. Hazard. Mater.* **2021**, *401*, 123813. [CrossRef] [PubMed]
290. Fahmy, A.; Elzaref, A.; Youssef, H.; Shehata, H.; Wassel, M.; Friedrich, J.; Poncin-Epaillard, F.; Debarnot, D. Plasma $O_2$ modifies the structure of synthetic zeolite-A to improve the removal of cadmium ions from aqueous solutions. *Turk. J. Chem.* **2019**, *43*, 172–184. [CrossRef]
291. Zhang, L.; Zhang, K.; Kang, S.; He, S.; Dong, X.; Zhao, Y.; Li, F.; Cen, Q. Study on using crystalline celluloses as templates for preparation of hierarchical LTA Zeolite for fast Cd(II) removal. *Chem. Eng. Res. Des.* **2023**, *200*, 32–41. [CrossRef]
292. Sai Krishna, G.V.; Matli, C.S. Synthesis and characterisation of pure zeolite A from fly ash for removal of lead and cadmium. *Int. J. Environ. Anal. Chem.* **2024**, 1–23. [CrossRef]
293. Nibou, D.; Mekatel, H.; Amokrane, S.; Barkat, M.; Trari, M. Adsorption of $Zn^{2+}$ ions onto NaA and NaX zeolites: Kinetic, equilibrium and thermodynamic studies. *J. Hazard. Mater.* **2010**, *173*, 637–646. [CrossRef] [PubMed]
294. El-Kamash, A.M.; Zaki, A.A.; El Geleel, M.A. Modeling batch kinetics and thermodynamics of zinc and cadmium ions removal from waste solutions using synthetic zeolite A. *J. Hazard. Mater.* **2005**, *127*, 211–220. [CrossRef]
295. Djamel, N.; Samira, A. Mechanism of $Cu^{2+}$ ions uptake process by synthetic NaA zeolite from aqueous solution: Characterization, kinetic, intra-crystalline diffusion and thermodynamic studies. *J. Mol. Liq.* **2021**, *323*, 114642. [CrossRef]
296. Cao, J.; Wang, P.; Shen, J.; Sun, Q. Core-shell Fe $_3O_4$@zeolite NaA as an adsorbent for $Cu^{2+}$. *Materials* **2020**, *13*, 5047. [CrossRef]

297. Buzukashvili, S.; Hu, W.; Sommerville, R.; Brooks, O.; Kökkılıç, O.; Rowson, N.A.; Ouzilleau, P.; Waters, K.E. Magnetic zeolite: Synthesis and copper adsorption followed by magnetic separation from treated water. *Crystals* **2023**, *13*, 1369. [CrossRef]
298. Huang, Y.; Li, M.; Guo, Y.; Ren, B.; Liu, X.; Zhu, L. A facile method to synthesize highly uniform zeolite A at near room temperature for copper (II) removal. *Mater. Today Commun.* **2022**, *30*, 103046. [CrossRef]
299. Li, J.; Li, M.; Song, Q.; Wang, S.; Cui, X.; Liu, F.; Liu, X. Efficient recovery of Cu(II) by LTA-zeolites with hierarchical pores and their resource utilization in electrochemical denitrification: Environmentally friendly design and reutilization of waste in water. *J. Hazard. Mater.* **2020**, *394*, 122554. [CrossRef] [PubMed]
300. Wang, C.; Zhou, J.; He, J.; Hao, C.; Pan, Y.; Meng, C. Synthesis of zeolite A and its application as a high-capacity cadmium ion exchanger. *Chin. J. Catal.* **2012**, *33*, 1862–1869.
301. Liu, J.; Huang, Z.; Sun, J.; Zou, Y.; Gong, B. Enhancing the removal performance of Cd(II) from aqueous solutions by NaA zeolite through doped thiourea reduced GO which is trapped within zeolite crystals. *J. Alloys Compd.* **2020**, *815*, 152514. [CrossRef]
302. Li, S.; Yang, Q.; Ye, Q.; Deng, X.; Su, Q.; Cui, X. Performance of metakaolin-based geopolymer molecular sieve microspheres on dynamic recovery of Cu (II). *Appl. Clay Sci.* **2024**, *255*, 107423. [CrossRef]
303. Al-Jubouri, S.M.; Holmes, S.M. Immobilization of cobalt ions using hierarchically porous 4A zeolite-based carbon composites: Ion-exchange and solidification. *J. Water Process Eng.* **2020**, *33*, 101059. [CrossRef]
304. Zhang, W.; Xu, F.; Wang, Y.; Luo, M.; Wang, D. Facile control of zeolite NaA dispersion into xanthan gum–alginate binary biopolymer network in improving hybrid composites for adsorptive removal of $Co^{2+}$ and $Ni^{2+}$. *Chem. Eng. J.* **2014**, *255*, 316–326. [CrossRef]
305. Abdelbaset, H.S.; Shama, S.A.; Hegazey, R.M.; Abdelrahman, E.A. Utilisation of wastes for low-cost synthesis of chitosan composites with nanosized sodium aluminium silicate hydrate and geopolymer/zeolite A for the removal of Hg(II) and Pb(II) ions from aqueous media. *Int. J. Environ. Anal. Chem.* **2023**, *103*, 182–200. [CrossRef]
306. Gao, M.; Yang, L.; Yang, S.; Jiang, T.; Wu, F.; Nagasaka, T. Simple aminated modified zeolite 4A synthesized using fly ash and its remediation of mercury contamination: Characteristics and mechanism. *Sustainability* **2022**, *14*, 15924. [CrossRef]
307. Jiang, C.; Yang, C.; Fu, Y.; Chen, F.; Hu, J. Highly efficient and selective Hg(II) adsorbent: ZnS grown on the surface of 4A zeolite and supported on starch aerogels. *Environ. Sci. Pollut. Res.* **2023**, *30*, 67059–67070. [CrossRef] [PubMed]
308. Wu, Z.; Chen, T.; Liu, H.; Wang, C.; Cheng, P.; Chen, D.; Xie, J. An insight into the comprehensive application of opal-palygorskite clay: Synthesis of 4A zeolite and uptake of $Hg^{2+}$. *Appl. Clay Sci.* **2018**, *165*, 103–111. [CrossRef]
309. Metaxas, M.; Kasselouri-Rigopoulou, V.; Galiatsatou, P.; Konstantopoulou, C.; Oikonomou, D. Thorium removal by different adsorbents. *J. Hazard. Mater.* **2003**, *97*, 71–82. [CrossRef] [PubMed]
310. Abbas, T.K.; Ibrahim, Z.H.; Mustafa, K.; Al-Juboori, R.A.; Nafae, T.M.; Al-Mashhadani, A.H.; Fal, M.; Alotaibi, A.M.; Alsalhy, Q.F. A modified zeolite ($Na_2SO_4$ @zeolite NaA) as a novel adsorbent for radium-226,228 from acidic radioactive wastewater: Synthesis, characterization and testing. *J. Environ. Chem. Eng.* **2024**, *12*, 112197. [CrossRef]
311. Hercigonja, R.V.; Vranješ-Djurić, S.D.; Mirković, M.D.; Marković, B.M.; Maksin, D.D.; Marković, B.N.; Nastasović, A.B. Technetium removal from the aqueous solution using zeolites A and Y containing transition metal ions $Co^{2+}$ and $Zn^{2+}$. *J. Radioanal. Nucl. Chem.* **2018**, *317*, 215–225. [CrossRef]
312. Nibou, D.; Khemaissia, S.; Amokrane, S.; Barkat, M.; Chegrouche, S.; Mellah, A. Removal of $UO_2^{2+}$ onto synthetic NaA zeolite. Characterization, equilibrium and kinetic studies. *Chem. Eng. J.* **2011**, *172*, 296–305. [CrossRef]
313. Barkat, M.; Nibou, D.; Amokrane, S.; Chegrouche, S.; Mellah, A. Uranium (VI) adsorption on synthesized 4A and P1 zeolites: Equilibrium, kinetic, and thermodynamic studies. *Comptes Rendus Chim.* **2015**, *18*, 261–269. [CrossRef]
314. Chostak, C.L.; López-Delgado, A.; Padilla, I.; Lapolli, F.R.; Lobo-Recio, M.Á. Agarose-immobilized LTA zeolite: A novel material to use in an improved treatment process of mine-impacted water. *Water Air Soil Pollut.* **2023**, *234*, 365. [CrossRef]
315. Jovanovic, M.; Arcon, I.; Kovac, J.; Tusar, N.N.; Obradovic, B.; Rajic, N. Removal of manganese in batch and fluidized bed systems using beads of zeolite a as adsorbent. *Microporous Mesoporous Mater.* **2016**, *226*, 378–385. [CrossRef]
316. Zayed, A.M.; Selim, A.Q.; Mohamed, E.A.; Abdel Wahed, M.S.M.; Seliem, M.K.; Sillanpää, M. Adsorption characteristics of Na-A zeolites synthesized from Egyptian kaolinite for manganese in aqueous solutions: Response surface modeling and optimization. *Appl. Clay Sci.* **2017**, *140*, 17–24. [CrossRef]
317. Yang, L.; Gao, M.; Wei, T.; Nagasaka, T. Synergistic removal of As(V) from aqueous solution by nanozero valent iron loaded with zeolite 5A synthesized from fly ash. *J. Hazard. Mater.* **2022**, *424*, 127428. [CrossRef] [PubMed]
318. Yang, X.; Yan, B.; Liu, Y.; Zhou, F.; Li, D.; Zhang, Z. Gamma-FeOOH based hierarchically porous zeolite monoliths for As(V) removal: Characterisation, adsorption and response surface methodology. *Microporous Mesoporous Mater.* **2020**, *308*, 110518. [CrossRef]
319. Mayta-Armas, A.F.; Canchanya-Huaman, Y.; Pomalaya-Velasco, J.; Bendezú-Roca, Y.; Checca-Huaman, N.-R.; Ramos-Guivar, J.A. Enhanced removal of As(V) and Pb(II) from drinking and irrigating water effluents using hydrothermally synthesized zeolite 5A. *Water* **2023**, *15*, 1892. [CrossRef]

320. Nasief, F.M.; Shaban, M.; Alamry, K.A.; Khadra, M.R.A.; Khan, A.A.P.; Asiri, A.M.; El-Salam, H.M.A. Hydrothermal synthesis and mechanically activated zeolite material for utilizing the removal of Ca/Mg from aqueous and raw groundwater. *J. Environ. Chem. Eng.* **2021**, *9*, 105834. [CrossRef]
321. El-Rahman, K.M.A.; El-Kamash, A.M.; El-Sourougy, M.R.; Abdel-Moniem, N.M. Thermodynamic modeling for the removal of $Cs^+$, $Sr^{2+}$, $Ca^{2+}$and $Mg^{2+}$ ions from aqueous waste solutions using zeolite A. *J. Radioanal. Nucl. Chem.* **2006**, *268*, 221–230. [CrossRef]
322. Soe, J.T.; Kim, S.-S.; Lee, Y.-R.; Ahn, J.-W.; Ahn, W.-S. $CO_2$ capture and $Ca^{2+}$ exchange using zeolite A and 13X prepared from power plant fly ash. *Bull. Korean Chem. Soc.* **2016**, *37*, 490–493. [CrossRef]
323. Song, J.; Liu, M.; Zhang, Y. Ion-exchange adsorption of calcium ions from water and geothermal water with modified zeolite A. *AIChE J.* **2015**, *61*, 640–654. [CrossRef]
324. Ma, D.; Wang, Z.; Guo, M.; Zhang, M.; Liu, J. Feasible conversion of solid waste bauxite tailings into highly crystalline 4A zeolite with valuable application. *Waste Manage.* **2014**, *34*, 2365–2372. [CrossRef] [PubMed]
325. Alcaraz, L.; Sotillo, B.; Iglesias, C.; López, F.A.; Fernández, P.; Belviso, C.; Urbieta, A. LTA zeolite particles functionalized with nanomagnetite for effective recovery of dysprosium from liquid solutions. *Microporous Mesoporous Mater.* **2024**, *363*, 112843. [CrossRef]
326. Malekpour, A.; Millani, M.R.; Kheirkhah, M. Synthesis and characterization of a NaA zeolite membrane and its applications for desalination of radioactive solutions. *Desalination* **2008**, *225*, 199–208. [CrossRef]
327. Mehdizadeh, S.; Sadjadi, S.; Ahmadi, S.J.; Outokesh, M. Removal of heavy metals from aqueous solution using platinum nanopartcles/zeolite-4A. *J. Environ. Health Sci. Eng.* **2014**, *12*, 7. [CrossRef] [PubMed]
328. Guaya, D.; Cobos, H.; Camacho, J.; López, C.M.; Valderrama, C.; Cortina, J.L. LTA and FAU-X iron-enriched zeolites: Use for phosphate removal from aqueous medium. *Materials* **2022**, *15*, 5418. [CrossRef] [PubMed]
329. Fouda, S.R.; Abd El Fattah, M.; Enew, A.M. The amputation of phosphate anions by cobalt oxide nanoparticles doped functionalized nanocomposites from wastewater. *Polyhedron* **2024**, *256*, 116994. [CrossRef]
330. Xiang, L.; Guo, Z.; Yang, L.; Qin, Y.; Chen, Z.; Wang, T.; Sun, W.; Wang, C. Modification of crystal growth of NaA zeolite with steric hindrance agents for removing ammonium ion from aqueous solution. *J. Ind. Eng. Chem.* **2024**, *132*, 326–334. [CrossRef]
331. Ham, K.; Kim, B.S.; Choi, K.-Y. Enhanced ammonium removal efficiency by ion exchange process of synthetic zeolite after $Na^+$ and heat pretreatment. *Water Sci. Technol.* **2018**, *78*, 1417–1425. [CrossRef]
332. Liu, H.; Peng, S.; Shu, L.; Chen, T.; Bao, T.; Frost, R.L. Effect of $Fe_3O_4$ addition on removal of ammonium by zeolite NaA. *J. Colloid Interface Sci.* **2013**, *390*, 204–210. [CrossRef] [PubMed]
333. Jiang, Z.; Yang, J.; Ma, H.; Ma, X.; Yuan, J. Synthesis of pure NaA zeolites from coal fly ashes for ammonium removal from aqueous solutions. *Clean Technol. Environ. Policy* **2016**, *18*, 629–637. [CrossRef]
334. Yang, K.; Zhang, X.; Chao, C.; Zhang, B.; Liu, J. In-situ preparation of NaA zeolite/chitosan porous hybrid beads for removal of ammonium from aqueous solution. *Carbohydr. Polym.* **2014**, *107*, 103–109. [CrossRef]
335. Shaban, M.; AbuKhadra, M.R.; Nasief, F.M.; Abd El-Salam, H.M. Removal of ammonia from aqueous solutions, ground water, and wastewater using mechanically activated clinoptilolite and synthetic zeolite-A: Kinetic and equilibrium studies. *Water Air Soil Pollut.* **2017**, *228*, 450. [CrossRef]
336. Kwakye-Awuah, B.; Labik, L.K.; Nkrumah, I.; Williams, C. Removal of ammonium ions by laboratory-synthesized zeolite Linde type A adsorption from water samples affected by mining activities in Ghana. *J. Water Health* **2013**, *12*, 151–160. [CrossRef] [PubMed]
337. Moussavi, G.; Talebi, S.; Farohki, M.; Mojtabaee Sabouti, R. Removal of ammonium from water by adsorption onto synthetic zeolites NaA and NaX: A comparative parametric, kinetic, and equilibrium study. *Desalin. Water Treat.* **2013**, *51*, 5710–5720. [CrossRef]
338. Watanabe, Y.; Yamada, H.; Tanaka, J.; Komatsu, Y.; Moriyoshi, Y. Ammonium ion exchange of synthetic zeolites: The effect of their open-window sizes, pore structures, and cation exchange capacities. *Sep. Sci. Technol.* **2005**, *39*, 2091–2104. [CrossRef]
339. Zavareh, S.; Farrokhzad, Z.; Darvishi, F. Modification of zeolite 4A for use as an adsorbent for glyphosate and as an antibacterial agent for water. *Ecotoxicol. Environ. Saf.* **2018**, *155*, 1–8. [CrossRef] [PubMed]
340. Belachew, N.; Hinsene, H. Preparation of zeolite 4A for adsorptive removal of methylene blue: Optimization, kinetics, isotherm, and mechanism study. *Silicon* **2022**, *14*, 1629–1641. [CrossRef]
341. Wang, C.; Li, J.; Wang, L.; Sun, X.; Huang, J. Adsorption of dye from wastewater by zeolites synthesized from fly ash: Kinetic and equilibrium studies. *Chin. J. Chem. Eng.* **2009**, *17*, 513–521. [CrossRef]
342. Sapawe, N.; Jalil, A.A.; Triwahyono, S.; Shah, M.I.A.; Jusoh, R.; Salleh, N.F.M.; Hameed, B.H.; Karim, A.H. Cost-effective microwave rapid synthesis of zeolite NaA for removal of methylene blue. *Chem. Eng. J.* **2013**, *229*, 388–398. [CrossRef]
343. Belviso, C.; Guerra, G.; Abdolrahimi, M.; Peddis, D.; Maraschi, F.; Cavalcante, F.; Ferretti, M.; Martucci, A.; Sturini, M. Efficiency in ofloxacin antibiotic water remediation by magnetic zeolites formed combining pure sources and wastes. *Processes* **2021**, *9*, 2137. [CrossRef]

344. Von-Kiti, E.; Oduro, W.O.; Animpong, M.A.; Ampomah-Benefo, K.; Boafo-Mensah, G.; Kwakye-Awuah, B.; Williams, C.D. Evidence of electronic influence in the adsorption of cationic and zwitterionic dyes on zeolites. *Heliyon* **2023**, *9*, e20049. [CrossRef] [PubMed]
345. Nešić, A.R.; Veličković, S.J.; Antonović, D.G. Modification of chitosan by zeolite A and adsorption of Bezactive Orange 16 from aqueous solution. *Composites Part B* **2013**, *53*, 145–151. [CrossRef]
346. Liu, X.; Guo, Y.; Zhang, C.; Huang, X.; Ma, K.; Zhang, Y. Preparation of graphene oxide/4A molecular sieve composite and evaluation of adsorption performance for Rhodamine B. *Sep. Purif. Technol.* **2022**, *286*, 120400. [CrossRef]
347. Al-dahri, T.; AbdulRazak, A.A.; Rohani, S. Preparation and characterization of Linde-type A zeolite (LTA) from coal fly ash by microwave-assisted synthesis method: Its application as adsorbent for removal of anionic dyes. *Int. J. Coal Prep. Util.* **2022**, *42*, 2064–2077. [CrossRef]
348. Yu, X.H.; Lü, H.L.; Zhou, G.W.; Zhou, L.G.; Zhang, Y.C. Absorption of methyl orange by modified fly zeolites. *Adv. Mater. Res.* **2012**, *476–478*, 1365–1369. [CrossRef]
349. Finish, N.; Ramos, P.; Borojovich, E.J.C.; Zeiri, O.; Amar, Y.; Gottlieb, M. Zeolite performance in removal of multicomponent heavy metal contamination from wastewater. *J. Hazard. Mater.* **2023**, *457*, 131784. [CrossRef] [PubMed]
350. Ibrahim, H.S.; Jamil, T.S.; Hegazy, E.Z. Application of zeolite prepared from Egyptian kaolin for the removal of heavy metals: II. Isotherm models. *J. Hazard. Mater.* **2010**, *182*, 842–847. [CrossRef] [PubMed]
351. Hui, K.S.; Chao, C.Y.H.; Kot, S.C. Removal of mixed heavy metal ions in wastewater by zeolite 4A and residual products from recycled coal fly ash. *J. Hazard. Mater.* **2005**, *127*, 89–101. [CrossRef] [PubMed]
352. Prelot, B.; Araïssi, M.; Gras, P.; Marchandeau, F.; Zajac, J. Contribution of calorimetry to the understanding of competitive adsorption of calcium, strontium, barium, and cadmium onto 4A type zeolite from two-metal aqueous solutions. *Thermochim. Acta* **2018**, *664*, 39–47. [CrossRef]
353. Araissi, M.; Ayed, I.; Elaloui, E.; Moussaoui, Y. Removal of barium and strontium from aqueous solution using zeolite 4A. *Water Sci. Technol.* **2015**, *73*, 1628–1636. [CrossRef] [PubMed]
354. Breck, D.W.; Eversole, W.G.; Milton, R.M.; Reed, T.B.; Thomas, T.L. Crystalline zeolites. I. The properties of a new synthetic zeolite, type A. *J. Am. Chem. Soc.* **1956**, *78*, 5963–5972. [CrossRef]
355. de Morais França, A.M.; Sousa, F.W.; Loiola, A.R.; de Luna, F.M.T.; Vidal, C.B.; do Nascimento, R.F. Study of $Cu^{2+}$, $Ni^{2+}$, and $Zn^{2+}$ competitive adsorption on synthetic zeolite: An experimental and theoretical approach. *Desalin. Water Treat.* **2021**, *227*, 263–277. [CrossRef]


**Disclaimer/Publisher's Note:** The statements, opinions and data contained in all publications are solely those of the individual author(s) and contributor(s) and not of MDPI and/or the editor(s). MDPI and/or the editor(s) disclaim responsibility for any injury to people or property resulting from any ideas, methods, instructions or products referred to in the content.